Supporting Information

Charge-Driven Tripod Somersault on DNA for Ratiometric Fluorescence Imaging of Small Molecules in Nucleus

Kang-Nan Wang, Qian Cao,* Liu-Yi Liu, Zi-Jian Zhao, Wenting Liu, Dan-Jie Zhou, Cai-Ping Tan, Wei Xia, Liang-Nian Ji and Zong-Wan Mao*

MOE Key Laboratory of Bioinorganic and Synthetic Chemistry, School of Chemistry, Sun Yat-Sen University, Guangzhou 510275, P. R. China.

Materials and measurements:

All starting materials were used as received from commercial sources unless otherwise indicated. Solvents were purified by standard procedures. 2–methyl-benzothiazole, methyl iodide, 4-formyltriphenylamine, N-bromosuccinimide, 4-pyridinylboronic acid, $Pd(PPh_3)_4$ were purchased from J&K Scientific Ltd. MTT (3-(4,5-dimethylthiazol-2-yl)-2,5-diphenyltetrazolium bromide, J&K Scientific Ltd.), DMSO (dimethyl sulfoxide, Sigma Aldrich), MTDR (Mito Tracker Deep Red, Life Technologies), LTDR (Lyso Tracker Deep Red, Life Technologies), Rhodamine 6G and Coumarin 307 (Sigma-Aldrich), HSA (Human Serum Albumin, Sigma Aldrich), JC-1 (5,5’,6,6‘-tetrachloro-1,1’,3,3’-tetraethylbenzimidazolylcarbocyanineiodide, Life Technologies), CCCP (carbonyl cyanide 3-chlorophenylhydrazone, Life Technologies), H2DCFDA (2',7'-dichlorodihydrofluorescein diacetate, Sigma Aldrich), PI (propidium iodide, Sigma Aldrich), and Hoechst 33342 (2'-(4-ethoxyphenyl)-5-(4-methyl-1-piperazinyl)-1H,3'H-2,5'-bibenzimidazole, Sigma Aldrich) were used as received. Solvents were purified and degassed by standard procedures. The tested compounds were dissolved in DMSO just before the experiments, and the final working concentration of DMSO was kept at 1% (v/v). High resolution mass spectrometer (HRMS) was recorded on a Thermo Finnigan MAT95XP spectrometer (USA). The quoted m/z values represented the major peaks in the isotopic distribution. Microanalysis of elements (C, H, S, and N) was carried out using an Elemental Vario EL CHNS analyzer (Germany). Nuclear magnetic resonance (NMR) spectra were recorded on a Bruker Avance III 400/500/600 MHz spectrometer (Germany). Shifts were referenced relative to the internal solvent signals. High-performed liquid chromatography (HPLC) were recorded on a LCMS-2020 (Shimadzu). UV/Vis spectra were recorded on a Varian Cary 300 spectrophotometer (USA). Steady-state emission spectra and lifetime measurements were conducted on a combined fluorescence lifetime and steady state spectrometer FLS 920 (Edinburgh Instruments Ltd, England). Cell imaging experiments were carried out on a confocal microscope (LSM 720 with Airyscan, ZEISS, Germany). Flow cytometric analysis was done using a BD FACS Calibur™ flow cytometer (Becton Dickinson, USA).

Synthesis and Characterization: As shown in Scheme S1 (ESI), 2-methyl-N-methyl-benzothiazolinium iodide (**S1**): **S1** was obtained by 2-methyl-benzothiazole and methyl iodide under 40 ^{o}C with ethanol as solvent.[1] 4-(Bis(4-bromophenyl)amino)benzaldehyde (**S2**): 4-formyltriphenylamine (5.46 g, 0.2 mol) was dissolved in dry THF (50 mL). NBS (N-bromosuccinimide) (9.26 g, 56 mmol, 2.6 eq.) was added in two times at room temperature, the whole process was carried out in nitrogen atmosphere. The mixture was stired for 1 hour at room temperature and then heated to reflux for 10 hours. The completion of the reaction was monitored by TLC. The solvent was then evaporated and excessive dichloromethane was added to the residue. The solid was filtered and washed with dichloromethane. The filtrate was washed with a 20% Na_2CO_3 aqueous solution and with water. The organic phase was dried with anhydrous sodium sulfate, filtered, and the solvent was removed by rotary evaporation. The residue was purified by column chromatography over silica gel (petroleum ether/chloroform, 1 **:** 2) to give **S2** (7.4 g, 87 %). ^{1}H NMR (400 MHz, DMSO) δ 9.82 (s, 1H), 7.77 (d, *J* = 8.8 Hz, 2H), 7.57 (d, *J* = 8.8 Hz, 4H), 7.11 (d, *J* = 8.8 Hz, 4H), 7.00 (d, *J* = 8.7 Hz, 2H). ^{13}C NMR (101 MHz, DMSO) δ 191.32 (s), 152.33 (s), 145.27 (s), 133.38 (s), 131.81 (s), 130.18 (s), 128.38 (s), 120.29 (s), 117.91 (s).

4-(Bis(4-(pyridin-4-yl)phenyl)amino)benzaldehyde (**S3**): The synthesis of compound **S3** followed the literature. [2, 3] **S2** (430 mg, 1 mmol), 4-pyridinylboronic acid (370 mg, 3.0 mmol), and K_2CO_3 (3.0 mmol, 3.0 ml, 1.0 mM) and $Pd(PPh_3)_4$ (20 mg, 0.054 mmol) were added in 1,4-dioxane (10 mL). The mixture was stirred at 110 ^{o}C under N_2 for 4 h, the mixture turns brown. Then the mixture was cooled to room temperature and poured into water. The organic phase was washed with saturated solution of NaCl and dried over sodium sulfate and the solvent was removed by rotary evaporation. After concentrated solution, precipitation is precipitated when a large amount of methanol is added into the oily product. The precipitate was washed with methanol to give **S3** (278 mg, 65%). ESI-MS (m/z): calcd. for $[M+H]^+$ ($C_{29}H_{21}N_3O$): 428.1685; found: 428.1772. ^{1}H NMR (500 MHz, $CDCl_3$) δ 9.89 (s, 1H), 8.67 (d, *J* = 6.1 Hz, 4H), 7.78 (d, *J* = 8.7 Hz, 2H), 7.65 (d, *J* = 8.6 Hz, 4H), 7.52 (d, *J* = 4.6 Hz, 4H), 7.30 (d, *J* = 8.6 Hz, 4H), 7.20 (d, *J* = 8.6 Hz, 2H). ^{13}C NMR (126 MHz, $CDCl_3$) δ 190.48 (s), 152.43

(s), 150.29 (s), 147.29 (s), 147.02 (s), 134.36 (s), 131.41 (s), 130.60 (s), 128.38 (s), 126.09 (s), 121.50 (s), 121.22 (s).

(E)-2-(4-(bis(4-(pyridin-4-yl)phenyl)amino)styryl)-3-methylbenzo[d]thiazol-3-ium iodide (**[PAST]**$^+$): **S1** (0.285 g，0.98 mmol) and **S2** (0.427 g, 1 mmol) were dissolved in ethanol and 3 drops of piperidine were added in turn. The reaction mixture was heater under reflux at 50 ^{o}C for 4 h. After cooling to room temperature, precipitate of compound **[PAST]**$^+$ was filtered under reduced pressure and washed by ethanol to get pure products without further purification. HRMS (m/z): calcd. for $[M-I]^+$ ($C_{38}H_{29}N_4S$): 573.21078; found: 573.21074. Elemental analysis: calcd (%) for $C_{38}H_{29}N_4SI$: C, 65.07; H, 4.15; N, 8.03; S, 4.61; found: C, 65.09; H, 4.17; N,8.01; S,4.59. ^{1}H NMR (400 MHz, DMSO) δ 8.64 (d, *J* = 6.1 Hz, 4H), 8.41 (d, *J* = 8.0 Hz, 1H), 8.22 (d, *J* = 8.5 Hz, 1H), 8.18 (d, *J* = 15.7 Hz, 1H), 8.01 (d, *J* = 8.8 Hz, 2H), 7.87 (m, *J* = 15.4, 8.6 Hz, 6H), 7.78 (d, *J* = 7.9 Hz, 1H), 7.74 (d, *J* = 6.2 Hz, 4H), 7.30 (d, *J* = 8.6 Hz, 4H), 7.15 (d, *J* = 8.7 Hz, 2H), 4.33 (s, 3H). ^{13}C NMR (101 MHz, DMSO) δ 172.20 (s), 150.63 (s), 148.64 (s), 147.06 (s), 146.61 (s), 142.50 (s), 133.66 (s), 132.29 (s), 129.76 (s), 128.78 (d, *J* = 25.6 Hz), 128.47 (s), 128.04 (s), 126.26 (s), 124.63 (s), 122.13 (s), 121.33 (s), 117.13 (s), 111.86 (s), 36.78 (s).

(Z)-1-(4-(bis(4-(pyridin-4-yl)phenyl)amino)phenyl)-2-(3-methylbenzo[d]thiazol-2(3H)-ylidene) ethanesulfonate (**[PAT]**$^-$): **[PAST]**$^+$ (0.527 g, 1.0 mmol) was dissolved in a mixture of methanol and water (1:1). Cautiously add, dropwise, Na_2SO_3 saturated aqueous solution (1.26 g, 10 mmol), allowing the reaction to subside between drops. The mixture reacted at room temperature for 4 h. The obtained yellow precipitate was filtrated, dried in vacuum. Finally, the crude product was purified by column chromatography using dichloromethane and methanol to give a yellow solid (0.176 g, 26.9%). HRMS (m/z): calcd. for $[M-H]^-$ ($C_{38}H_{29}N_4O_3S_2$): 653.1687; found: 653.1693. Elemental analysis: calcd (%) for $C_{38}H_{29}N_4O_3S_2.1.5H_2O$: C, 66.94; H, 4.88; N, 8.23; S, 9.41; found: C, 66.93; H, 4.87; N,8.25; S,9.37. ^{1}H NMR (500 MHz, DMSO) δ 8.66 (s, 4H), 8.13 (s, 1H), 7.85 – 7.74 (m, 8H), 7.34 (d, *J* = 8.3 Hz, 2H), 7.31 (d, *J* = 8.3 Hz, 1H), 7.26 (d, *J* = 7.7 Hz, 1H), 7.23 (d, *J* = 8.3 Hz, 1H), 7.13 (d, *J* = 8.6 Hz, 4H), 7.04 (d, *J* = 7.4 Hz, 1H), 7.01 (d, *J* = 8.3 Hz, 2H), 6.52 (s, 1H), 3.34 (s, 3H). ^{13}C NMR (126 MHz, DMSO) δ 165.60 (s), 163.50 (s), 149.82 (s), 148.46 (s), 147.48 (s), 145.14 (s), 140.12 (s), 133.59

(s), 131.64 (s), 131.11 (s), 128.81 (s),128.62 (s), 127.81 (s), 125.00 (s), 123.74 (s), 123,32 (s), 121.55, 117.81 (s), 62.70 (s), 45.59 (s), 32.70 (s).

Crystallographic structure determination

Single crystals of **[PAST]$^+$** qualified for X-ray analysis were obtained by diffusion of diethyl ether to the mixture solutions of CH_2Cl_2. X-ray diffraction measurements were performed on a Brucker Smart 1000 CCD diffractometer with Cu Kα radiation (λ = 1.54178 Å) at 50(2) K the crystal structures of **[PAST]$^+$** was solved by direct methods with program SHELXS and refined using the full-matrix least-squares program SHELXL.4 Crystallographic data and details of data collection and structure refinements are listed in Table S1. Selected bond distances and angles are listed in Table S2-S3. The structural plots were drawn using the xp package in SHELXL at a 30% thermal ellipsoids probability level.

Measurements of absorption and emission spectra: The spectroscopic investigations were carried out in PBS (pH=7.4), CH_3OH and CH_2Cl_2 used without further purification. The absorption spectra were recorded with a Varian Cary 300 spectrophotometer at 298K. The emission spectra were recorded on an Edinburgh FLS 920 Spectrometer at 298K. The analysis of the luminescence decay profiles was accomplished with decay-analysis software provided by the manufacturer, and the quality of the fit was assessed with the χ^2 value close to unity and with the residuals regularly distributed along the time axis. Stock solutions of **[PAST]$^+$** and **[PAT]$^-$** (20 mM) were prepared in DMSO and diluted to the indicated concentrations by PBS. Other analytes ($S_2O_8^{2-}$, SO_4^{2-}, HS^-, H_2O_2, $C_2O_4^-$, ClO^-, ClO_4^-, NO, NO_2^-, NO_3^-, NH_4^+ Cys, GSH, EDTA, Citric acid, HPO_4^{2-}, F^-, Cl^-, HCO_3^-, OH^-, $C_2O_4^{2-}$, CN^-, CH_3COO^-) were prepared in twice distilled water at 2 mM. Data analysis was performed using GraphPad Prism 7.00.

Spectroscopic response of [PAST]$^+$ to HSO_3^- in aqueous solution: UV-Vis and fluorescence titration experiments were performed by incubating 10 μM of the **[PAST]$^+$** with varying concentrations of HSO_3^- aqueous solution (pH 7.4, 20 mM PBS buffer) at 25 ^oC for 2 min, and the spectral changes were monitored versus HSO_3^- concentration. The time dependence of the response of **[PAST]$^+$** (10 μM) to HSO_3^- were

determined in PBS by monitoring the fluorescence changes (λ_{em} = 735 nm) versus incubation time.

Spectroscopic response of $[PAST]^+$ to HSO_3^- in DNA enrichment buffer: Fluorescence titration experiments were performed by incubating 10 μM of **$[PAST]^+$** with varying concentrations of 12-mer duplex DNA (dsDNA) or calf thymus DNA (ctDNA) in PBS, and the spectral changes completed when the concentration of ds DNA was higher than 6 μM or the concentration of ctDNA was higher than 40 μg/mL. Therefore, DNA enrichment buffer was prepared by adding 6 μM dsDNA or 40 μg/mL ctDNA in PBS. Then UV-Vis and fluorescence titration experiments were performed by incubating 10 μM of the **$[PAST]^+$** with varying concentrations of HSO_3^-in such DNA enrichment buffer, and the spectral changes were monitored versus HSO_3^- concentration.

Circular dichroism (CD) spectroscopy. CD spectra were measured using a J-810 spectropolarimeter (JASCO, Japan) with a wavelength range of 200–400 nm, 1 cm optical path-length, and 200 nm/min scan speed at room temperature. The dsDNA samples were dissolved in Phosphate-buffered saline (pH = 7.4). The concentration of DNA samples was 5 μM. After each addition of the **$[PAST]^+$** and **$[PAT]^-$**, the solution was stirred and allowed to equilibrate for at least 10 min.

NMR experiments. All NMR experiments were performed on the Bruker AVIII 400/600 MHz spectrometers. PBS contained 8 mM Na_2HPO_4, 1 mM KH_2PO_4, 137 mM NaCl, and 3 mM KCl (pH = 7.4) in D_2O/H_2O (v/v 1:9) were used to prepare DNA samples. The final concentrations of DNA samples were 0.1–2.5 mM. 2D NMR experiments were collected at different temperatures of 5°C in H_2O and D_2O solutions. The mixing times of NOESY were set from 50–300 ms. Peak assignments and integrations were made using Sparky (UCSF). WATERGATE or presaturation water suppression techniques were used for water NMR samples.

Structure preparation and molecular docking: The 3D structure of the DNA-ligand complex was downloaded from RCSB Protein Data Bank (PDB code: 1QSX) and prepared with the default structure preparation workflow in Schrodinger fix issues like

missing atoms and/or non-standard atom names, etc. After that, the original ligand was replaced by our target compounds with the use of the glide docking algorithm.

The protonation state of the DNA and the orientation of the hydrogens were optimized by Schordinger, at the pH of 7 and temperature of 300 K. Glide docking 8 was used for docking ligands (including the substrate and the product) to the DNA system following the "induced fit" protocol. The docked poses were ranked by XP scoring and different binding modes are chosen artificially for the following MD simulations. Eventually, 4 substrate-DNA complexes and 4 product-DNA complexes were selected for the next MD simulations.

The ligand-DNA complex was then neutralized by adding sodium/chlorine counter ions, and solvated in a cuboid box of TIP3P [4] water molecules with solvent layers 10 Å between the box edges and solute surface, neutralized by adding sodium/chlorine counter ions. The ligands were first optimized by Gaussian09 package [5] at the level of B3LYP/6-31g*. Then the partial atomic charges were calculated by the restrained electrostatic potential (RESP) [6] charge from the calculation with Gaussian09 package at HF/6-31g* level.

Molecular dynamics simulations: All MD simulations were performed using AMBER 16. [7, 8] The AMBER GAFF and BSC1 force fields were applied to describe the ligands and DNA system. The whole system was minimized with 10000 steps, then the Langevin thermostat was employed to heat up the system to 300K. [9] After that, the Berenson barostat was used to equilibrate the density. The long time simulations are based on the equilibrated structure. During the simulations, the SHAKE algorithm was used to restrict all covalent bonds involving hydrogen atoms with a time step of 2 fs. The Particle mesh Ewald (PME) method [10] was employed to treat long-range electrostatic interactions. Totally 100 ns simulations were carried out for each conformation and the trajectories were further analyzed using Cpptraj in Amber16.

Cell lines and culture conditions: A549 cells were obtained from Experimental Animal Center of Guangzhou Cell cook Biotech Co., ltd (Guangzhou, China), PC-3 and HeLa cells were obtained from Shanghai Zhong Qiao Xin Zhou Biotechnology Co., Ltd.

(Shanghai, China). Cells were routinely maintained in DMEM (Dulbecco's modified Eagle's medium, Gibco BRL) or RPMI 1640 (Roswell Park MemorialInstitute 1640, Gibco BRL) medium containing 10% FBS (fetal bovine serum, Gibco BRL), 100 μg/mL streptomycin, and 100 U/mL penicillin (Gibco BRL). The cells were cultured in tissue culture flasks in a humidified incubator at 37 °C, in an atmosphere of 5% CO_2 and 95% air. In each experiment, the cells treated with vehicle DMSO (1%, v/v) were used as the referent group.

Cytotoxicity assay: Cells cultured in 96-well plates were grown to confluence. The compounds were dissolved in DMSO (1%, v/v), and diluted with fresh media immediately. Then the cells were incubated with different concentrations of the tested compounds for 2 or 20 h at 37 °C. 20 mL of MTT solution was then added to each well, and the plates were incubated for an additional 4 h. The medium was carefully removed, and DMSO was added (150 μL per well). The plates were incubated for 10 min with shaking. The absorbance at 595 nm was measured using a microplate reader (Infinite M200 Pro, Tecan, Switzerland).

Cellular localization assay: A549 cells were seeded into 35 mm dishes (Greiner, Germany) for confocal microscopy. After cultured two days, the cells were incubated with **[PAST]$^+$** at 20.0 μM for 20 min. The treated cells were observed immediately under a confocal microscope. For colocalization studies, the cells were incubated with **[PAST]$^+$** (20.0 μM) for 20 min. Subsequently, the medium was replaced with staining medium containing Hoechst33342 (150 nM), MTDR, LDTR (100 nM) and stained for another 30 min. The cells were washed twice with PBS, and then viewed immediately under a confocal microscope. The cells were analyzed immediately by confocal microscopy with excitation at 405 nm and emission at 460 ± 20 nm for Hoechst33342, and with excitation at 633 nm and emission at 650 ± 20 nm for MTDR and LTDR, respectively.

Ratiometric fluorescence imaging: A549 cells were seeded into 35 mm dishes and cultured for two days. Before treatment with probe, cells were simulated with various concentrations of thiosulphate/GSH (2:1) for 30 min to induce different amounts of endogenous SO_2 derivatives. Then cells were incubated with **[PAST]$^+$** at 20 μM for

another 20 min and ratiometric fluorescence imaging were obtained with a dual-emission mode (λ_{ex} = 405 nm) by mediating the yellow channel image (band path of 565 ± 20 nm) with the corresponding red channel image (band path of 665 ± 20 nm).

Cell fixation and permeability treatment: A549 cells were seeded into 35 mm dishes and incubated for 48 h and then treated with **[PAT]**$^-$ for 20 min. The cells were then washed twice with cold PBS and fixed with 4% paraformaldehyde at room temperature for 10 min. After washed with cold PBS, the cells were analyzed immediately by confocal microscopy with excitation at 405 nm and emission at 565 ± 20 nm.

Nuclease treatment: A549 cells were fixed in 75% ethanol for 1 h and permeablized with 1% TritonX-100 in PBS for 30 min. And then A549 cells were washed with PBS (pH = 7.4) twice. For Nuclease digest test, 100 μg/mL Nuclease was added into two sets of prefixed A549 cells for 30 min. And then cells were stained with 20.0 μM **[PAST]**$^+$ in PBS (pH = 7.4) for 20 min. After rinsing with PBS, a total 1 mL PBS (as control experiment) was added into one of the set of A549 cells digested by Nuclease. 200 μM $NaHSO_3$was added into another set of cells for 30 min. Cells were rinsed by clean PBS twice before imaging.

Analysis of MMP by confocal microscopy: A549 cells were seeded into 35 mm dishes and treated with **[PAST]**$^+$ at the indicated concentrations for 6 h. After stained with JC-1, the cells were visualized by a confocal microscope with excitation at 488 nm. Fluorescence was monitored by measuring both the monomer (530 ± 20 nm; green) and the aggregate (590 ± 20 nm; red) forms of JC-1. A commercial drug can induce mitochondrial apoptosis CCCP as positive control.

Intracellular ROS detection by flow cytometry: the capability of **[PAST]**$^+$ to induce intracellular ROS elevation was examined by using flow cytometry. After treated with **[PAST]**$^+$ at the indicated concentrations (10 μM, 20 μM) for 6/12h, the cells were harvested and incubated with H_2DCFDA (2',7'-dichlorofluorescein diacetate, 10 μM) staining for 15 min at 37 °C in the dark. Cells were collected by centrifugation and

washed twice with PBS and serum-free medium to remove the excess staining dye. The fluorescence intensity of cells was measured immediately by flow cytometry with excitation at 488 nm and emission at 530 ± 30 nm. The MFI was analyzed using FlowJo 7.6 software (Tree Star, OR, USA). 10, 000 cells were acquired for each sample.

In vivo fluorescence imaging: Nude mice were obtained from the Guangdong Experimental Animal Center. All procedures adhered to the guidelines for the care and use of laboratory animals and were approved by the Institutional Animal Care Committee. Fluorescence imaging was performed on a small animal in vivo fluorescence imaging system (In-Vivo FxPro; Carestream, MI, USA) immediately after MR imaging. White light imaging, fluorescence imaging with 430 nm / 530 nm excitation wavelength and 600 nm / 700 nm emission wavelength were obtained. The fluorescence intensity in the in vivo imaging tests was quantified using the Care stream MI software.

Statistical analysis: All biological experiments were performed at least twice with triplicates in each experiment. Representative results were depicted in this report and data were presented as means ± standard deviations (SD) with statistical significance. [11] **$P < 0.05$, *$P < 0.02$.

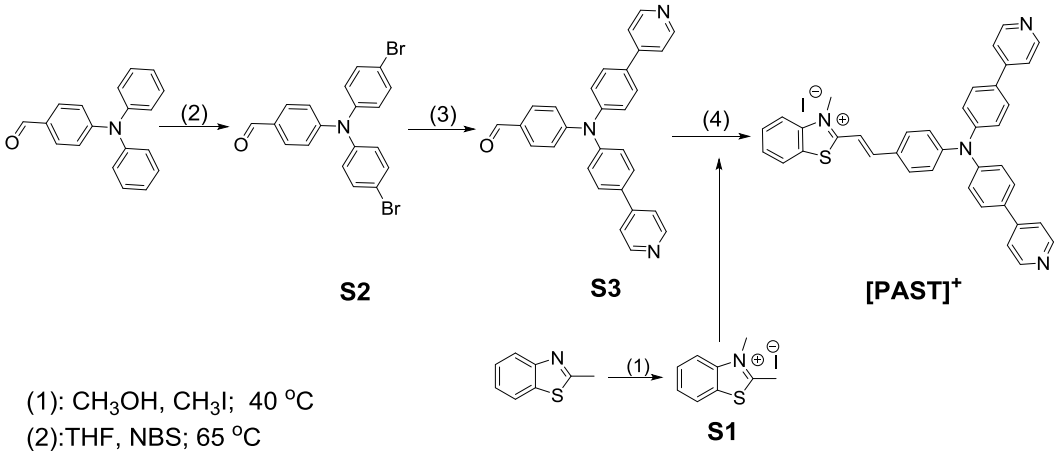

(1): CH_3OH, CH_3I; 40 °C
(2):THF, NBS; 65 °C
(3): $Pd(PPh_3)_4$, 4-Pyridylboronic acid, K_2CO_3, 1,4-dioxane; 110 °C
(4): C_2H_5OH, Piperidine; 72 °C

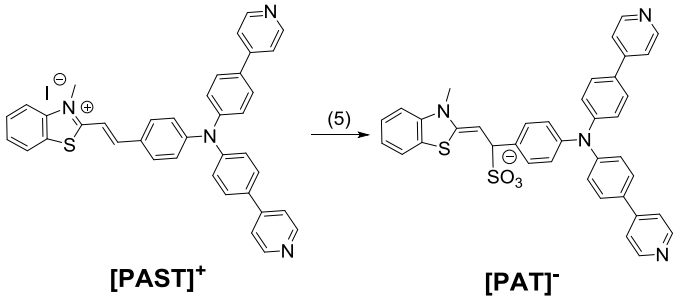

(5): CH_3OH, H_2O, $NaHSO_3$; 50 °C

Scheme S1. Synthetic routes of the compounds **[PAST]**$^+$ and **[PAT]**$^-$ in this work.

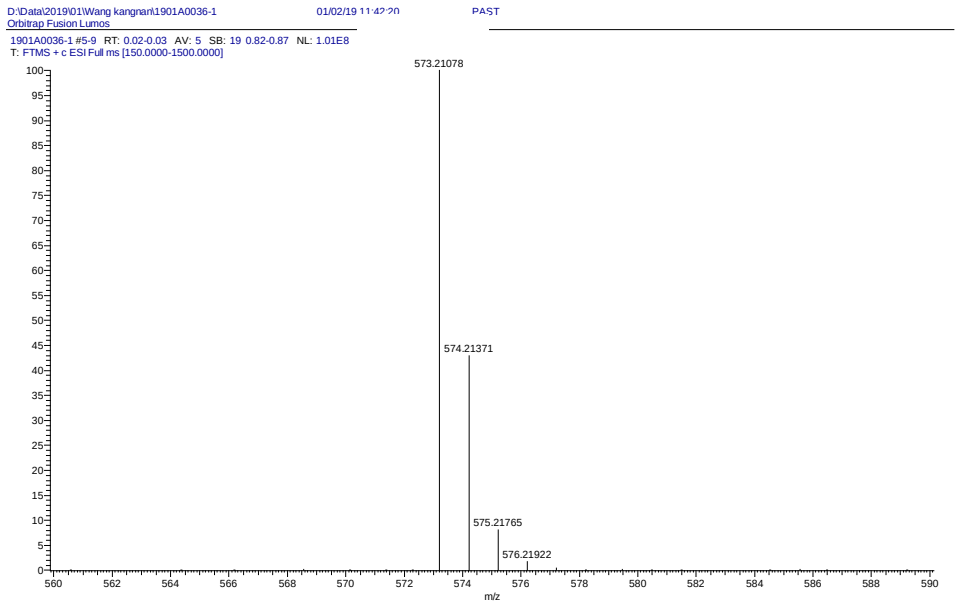

Fig. S1 HRMS spectrum of **[PAST]**$^{+}$.

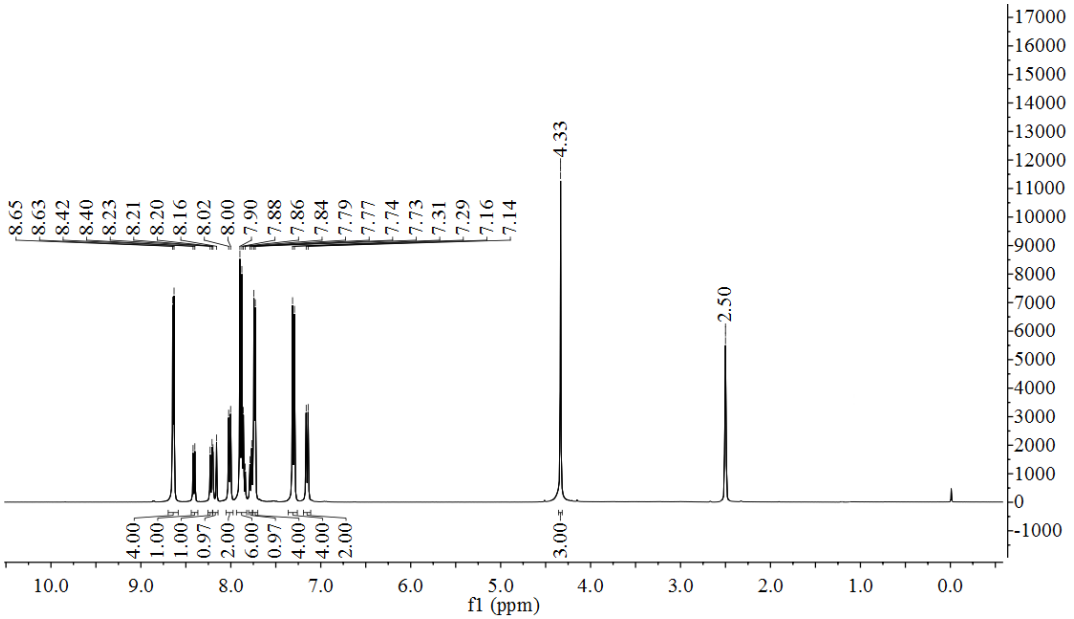

Fig. S2 ^{1}H NMR spectrum of **[PAST]**$^{+}$ in DMSO-d_6.

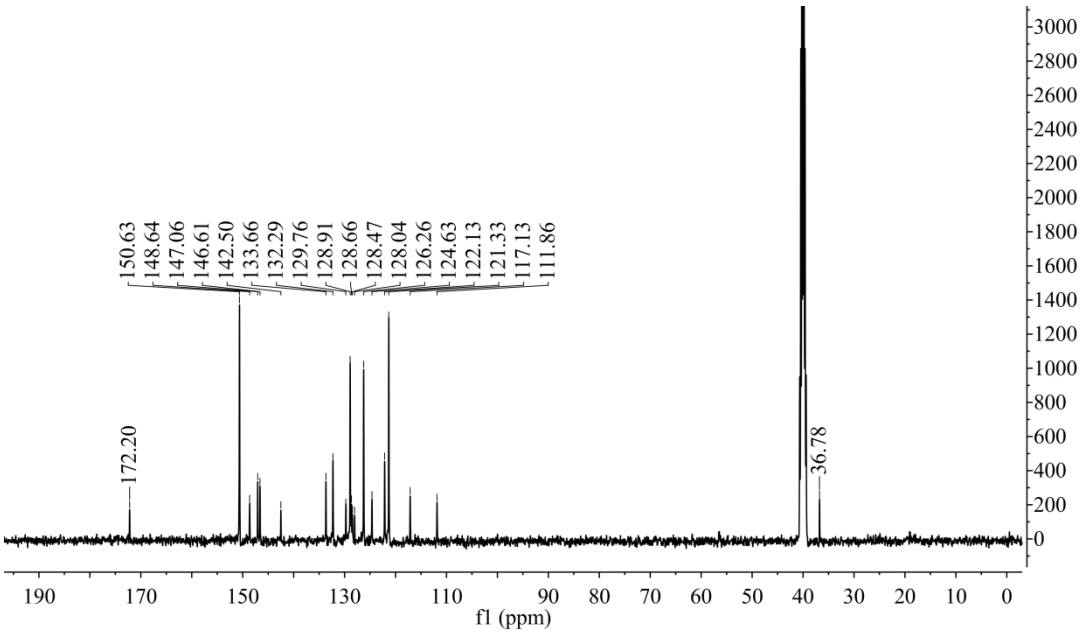

Fig. S3 ^{13}C NMR spectrum of **[PAST]**$^{+}$ in DMSO-d_6.

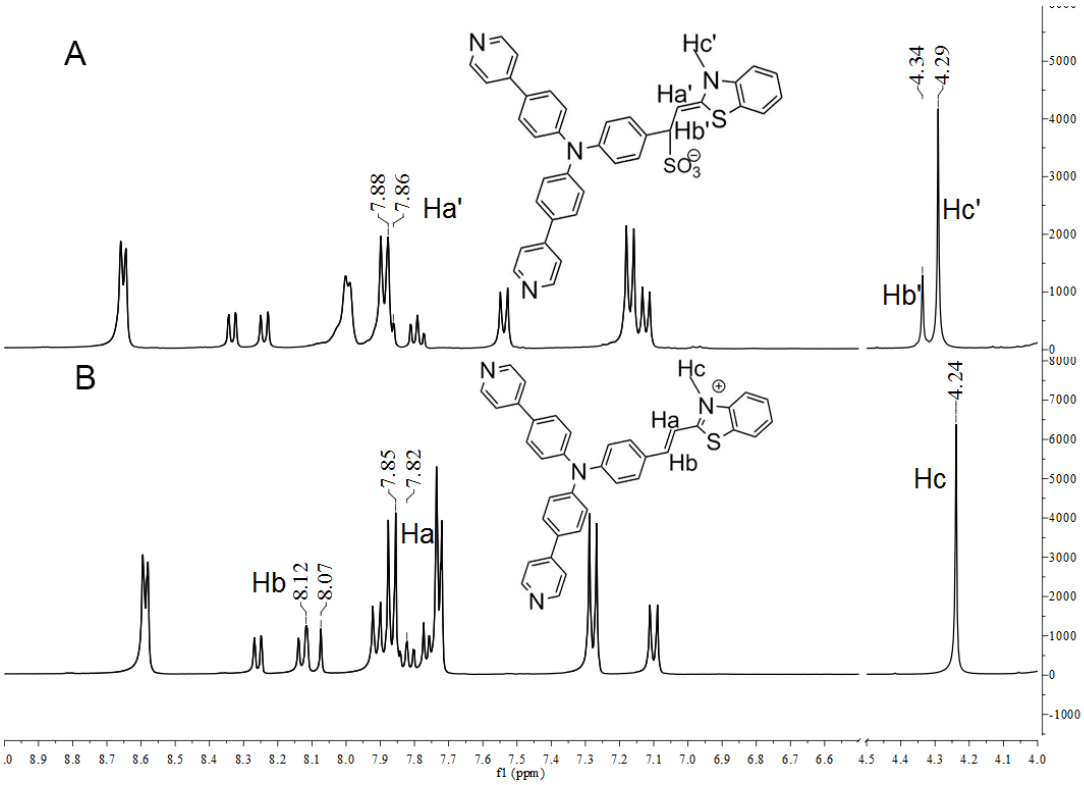

Fig. S4 Partial ^{1}H NMR spectra of probe **[PAST]**$^{+}$ (B) and **[PAT]**$^{-}$ (A) in DMSO-d_6-D_2O (4:1).

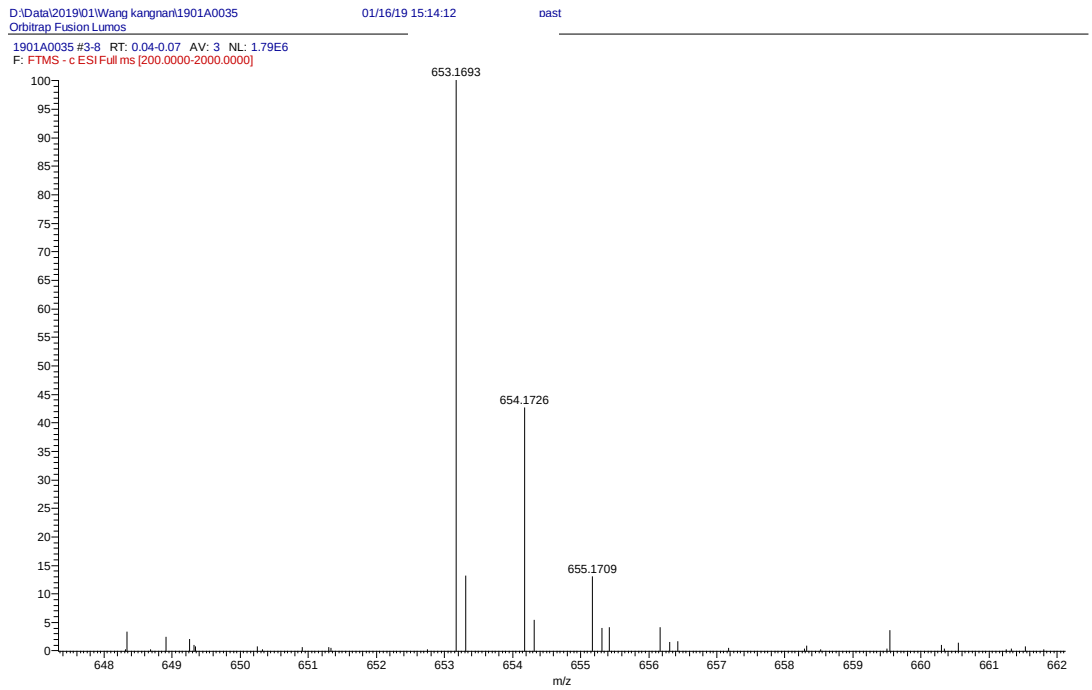

Fig. S5 HRMS spectrum of **[PAT]**$^{-}$.

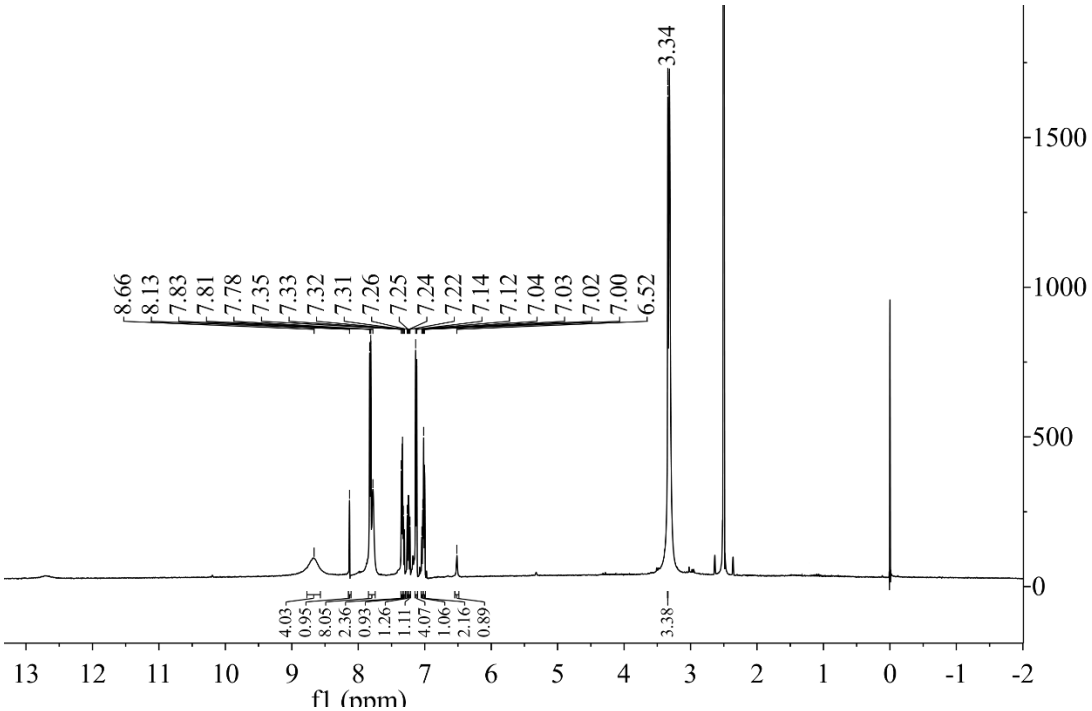

Fig. S6 ^{1}H NMR spectrum of **[PAT]**$^{-}$ in DMSO-*d6*. Solvent signals from H_2O were present at δ 3.33.

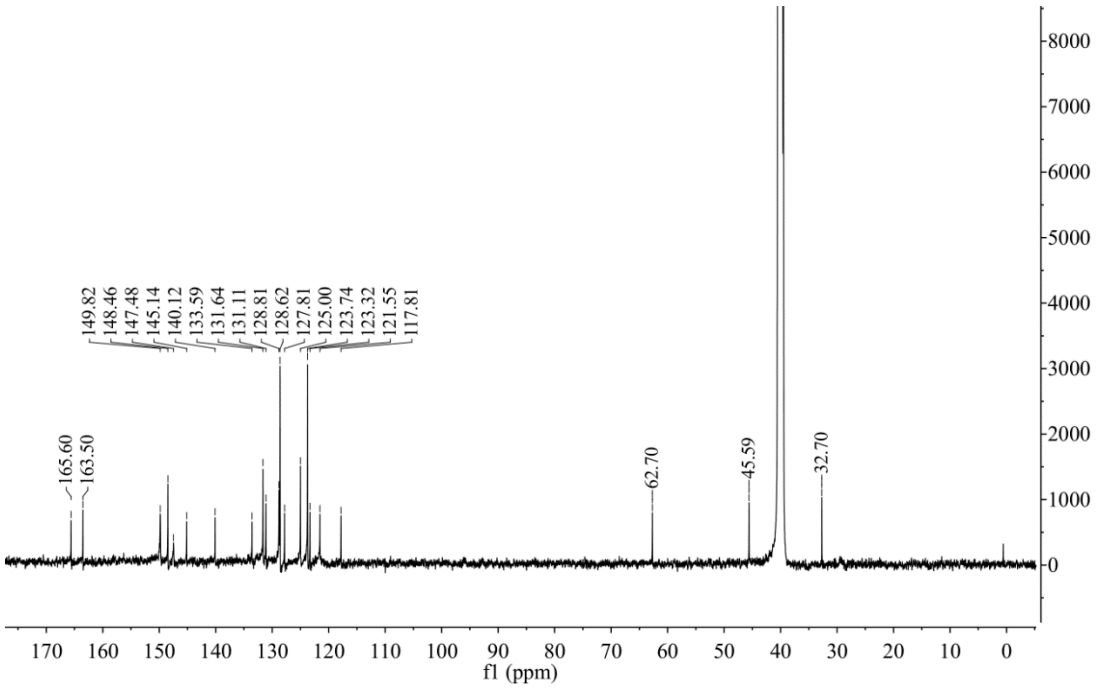

Fig. S7 ^{13}C NMR spectrum of **[PAT]**$^{-}$in DMSO-*d6*.

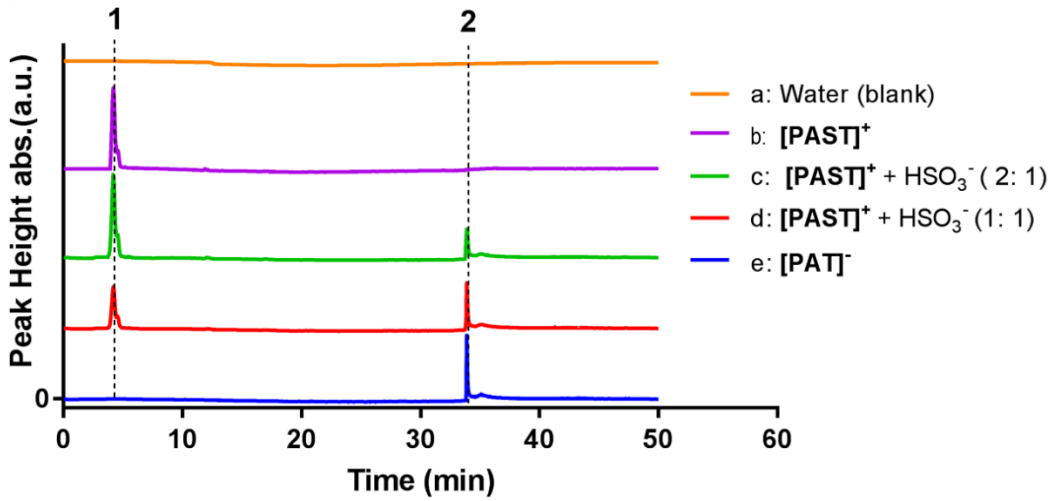

Fig. S8 HPLC trace of the addition reaction. (a) Water (blank); (b) pure **[PAST]**$^{+}$ (10 μM); (c) Reaction solution of **[PAST]**$^{+}$ (10 μM, 50 μL) with HSO_3^- (10 μM, 25 μL) for 10 min; (d) Reaction solution of **[PAST]**$^{+}$ (10 μM, 50 μL) with HSO_3^- (10 μM, 50 μL) for 10 min; (e) isolated pure **[PAT]**$^{-}$ (10 μM). Assignments of the peaks: (1) 4.21 min, **[PAST]**$^{+}$; (2) 33.89 min, **[PAT]**$^{-}$. The chromatographic peaks were monitored at 370 nm with acetonitrile: water (containing 0.1% formic acid) = 5 : 95 (flow rate, 0.6 mL/min) as eluent.

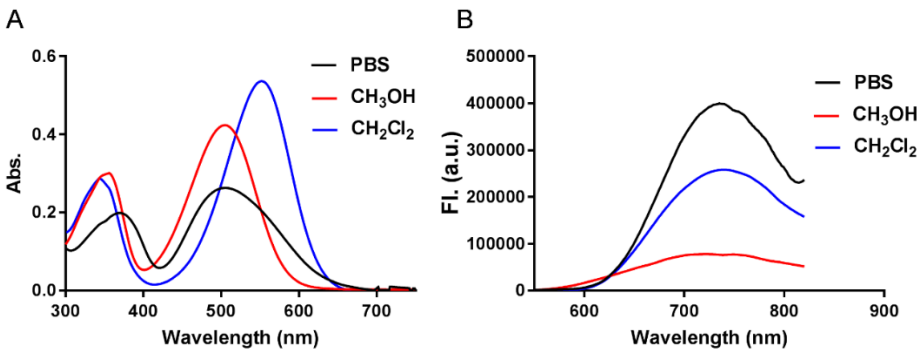

Fig. S9 UV-Vis absorption (A) and emission spectra (B) of **[PAST]**$^{+}$ (10 μM) measured in PBS (pH = 7.4), CH_3OH and CH_2Cl_2 at 298 K.

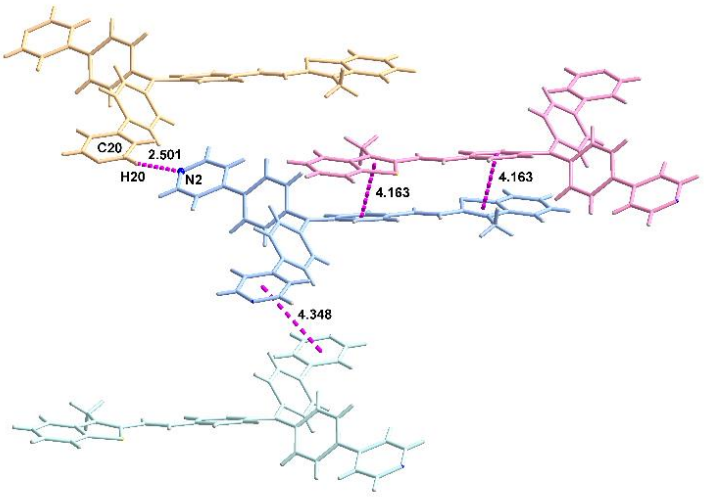

Fig. S10 The molecule of **[PAST]**$^{+}$ stack in dimers between nearest neighbors.

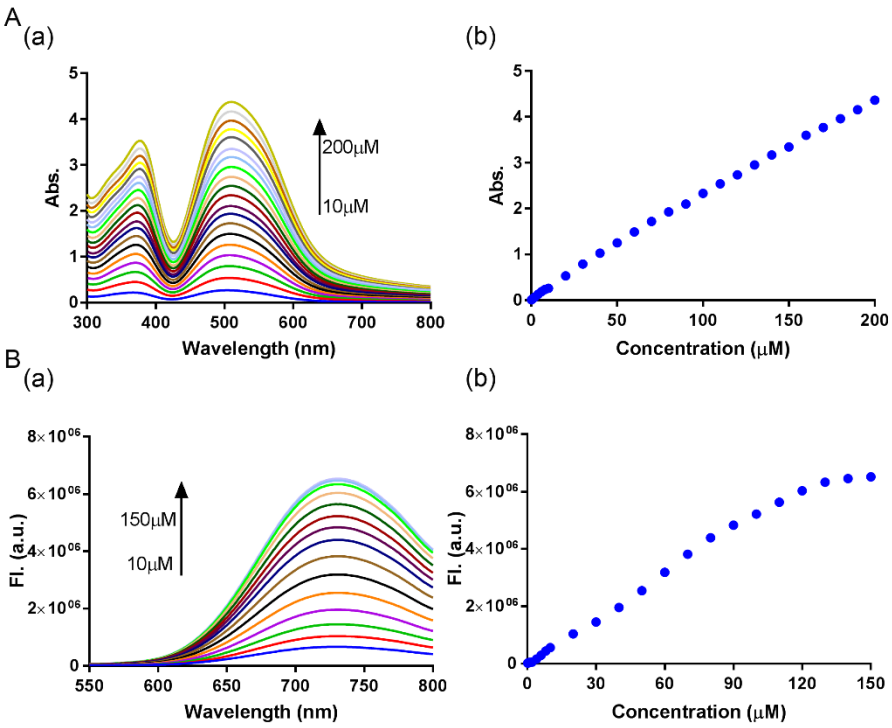

Fig. S11 (A) UV-Vis absorption spectra of **[PAST]**$^{+}$ at indicated concentrations (a: 10~200 μM in PBS) and the changes of the absorbanceat 515 nm as a function of **[PAST]**$^{+}$ concentrations (b: 0.1 μM~200 μM); (B) Emission spectra of **[PAST]**$^{+}$ at indicated concentrations (a: 10~150 μM in PBS) and the changes of the emission intensity at 735 nm as a function of **[PAST]**$^{+}$ concentrations(b: 0.1 μM~150 μM), λ_{ex} = 515 nm.

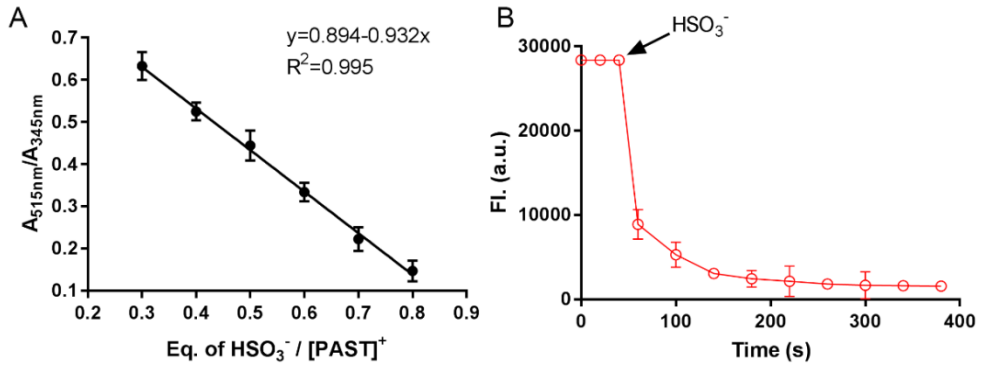

Fig. S12 (A) The linear relationship between the absorbance ratio A_{515}/A_{345} nm of **[PAST]**$^{+}$ (10 μM) and the concentration of $NaHSO_3$ in PBS solution (pH = 7.4); (B) Time course of the fluorescence response of **[PAST]**$^{+}$ (10 μM) upon the addition of 10 μM of $NaHSO_3$ in PBS (pH 7.4).

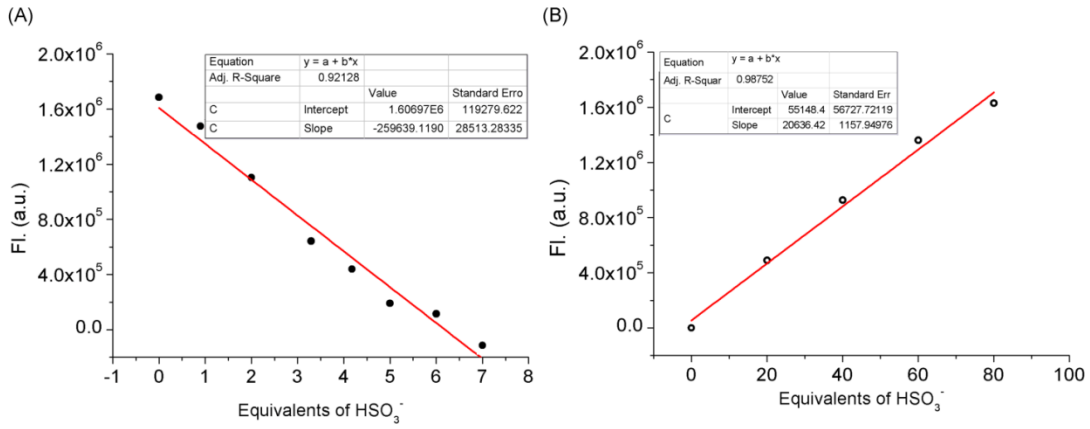

Fig. 13 Benesi-Hilderbr and plot of **[PAST]**$^{+}$ with SO_2 derivatives in PBS (A) or in DNA enrichment environment (B). (The detection limit DL of **[PAST]**$^{+}$ for SO_2 derivatives was determined from the following equation: *DL*=K*Sb1/S, Where K = 2 or 3; Sb1 is the standard deviation of the blank solution; S is the slope of the calibration curve.)

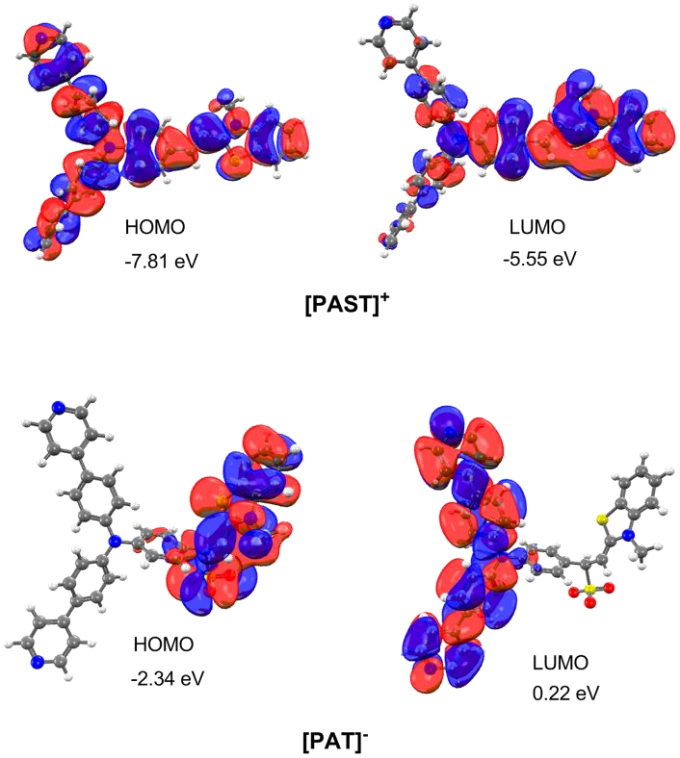

Fig. 14 Frontier molecular orbital plots of **[PAST]**$^{+}$ and **[PAT]**$^{-}$. Blue and red shapes are corresponding to the different phases of the molecular wave functions for HOMO and LUMO orbitals.

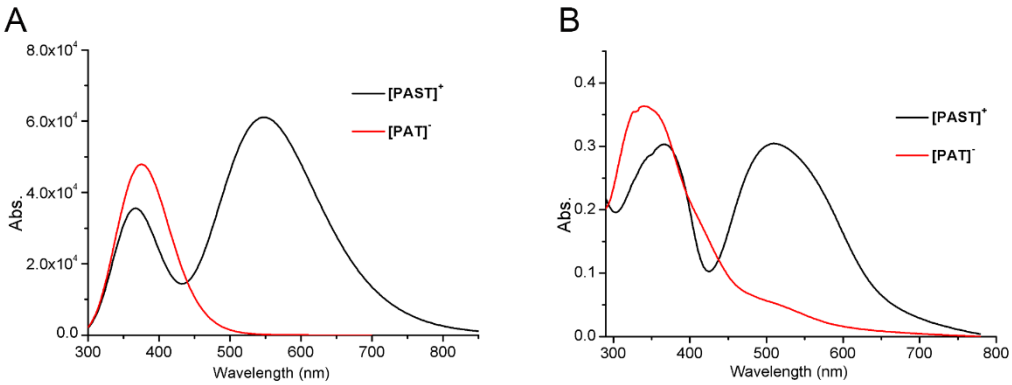

Fig. 15 Calculated absorption spectra (A) and experimental absorption spectra (B) of **[PAST]**$^{+}$ and **[PAT]**$^{-}$ in PBS.

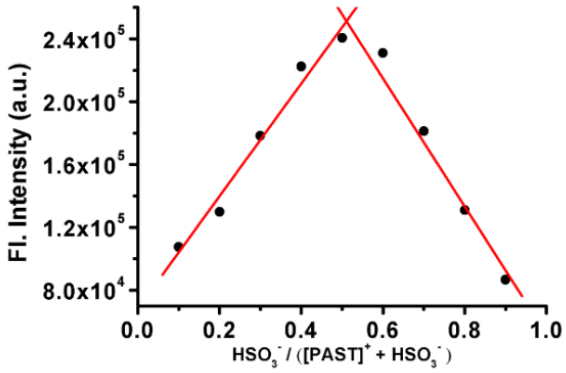

Fig. S16 Job plots for **[PAST]**$^{+}$ and sulfite interaction with a total concentration of **[PAST]**$^{+}$ + HSO_3^- at 10 μM by fluorescence measurement. λ_{ex} = 515 nm; λ_{em} = 735 nm.

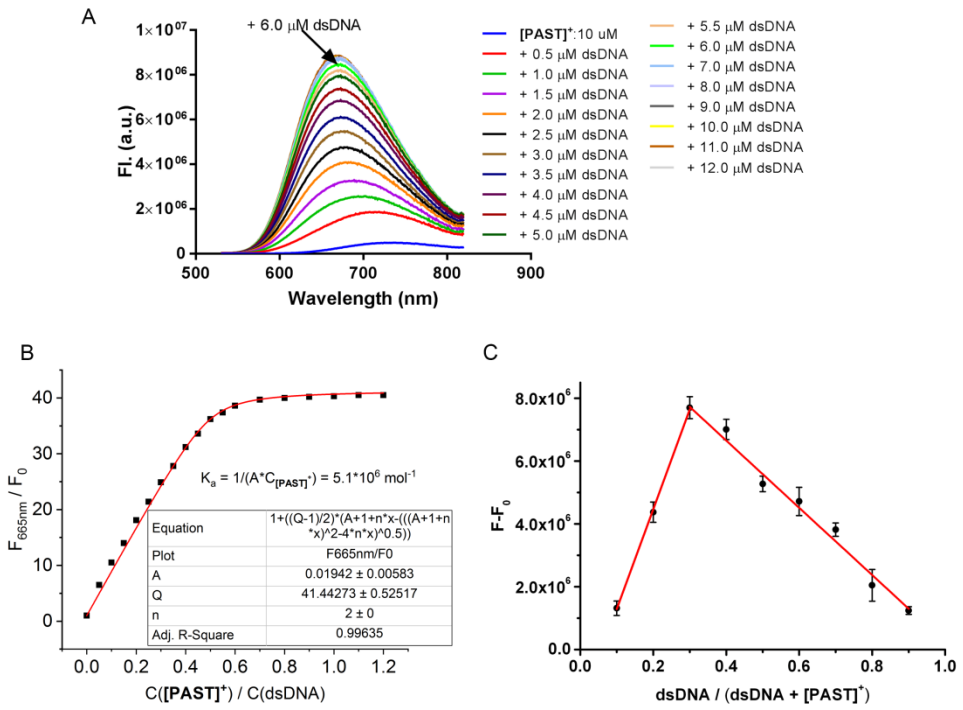

Fig. S17 (A) Fluorescence spectra of **[PAST]**$^{+}$ (10 μM) in PBS with increasing concentrations of dsDNA; (B) Binding constant of dsDNA and **[PAST]**$^{+}$ by fluorescence measurement; (C) Job plots for dsDNA and **[PAST]**$^{+}$ interaction with a total concentration of dsDNA + **[PAST]**$^{+}$ at 10 μM.

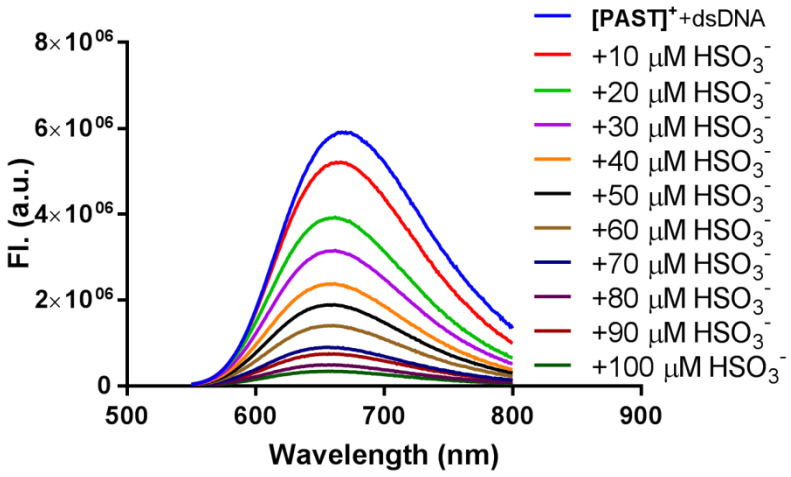

Fig. S18 Fluorescence response of **[PAST]**$^{+}$ (10 μM) toward different concentrations of $NaHSO_3$ (0-100 μM) in nucleic acid enrichment buffer solution (PBS with 6 μM of dsDNA) λ_{ex} = 515 nm.

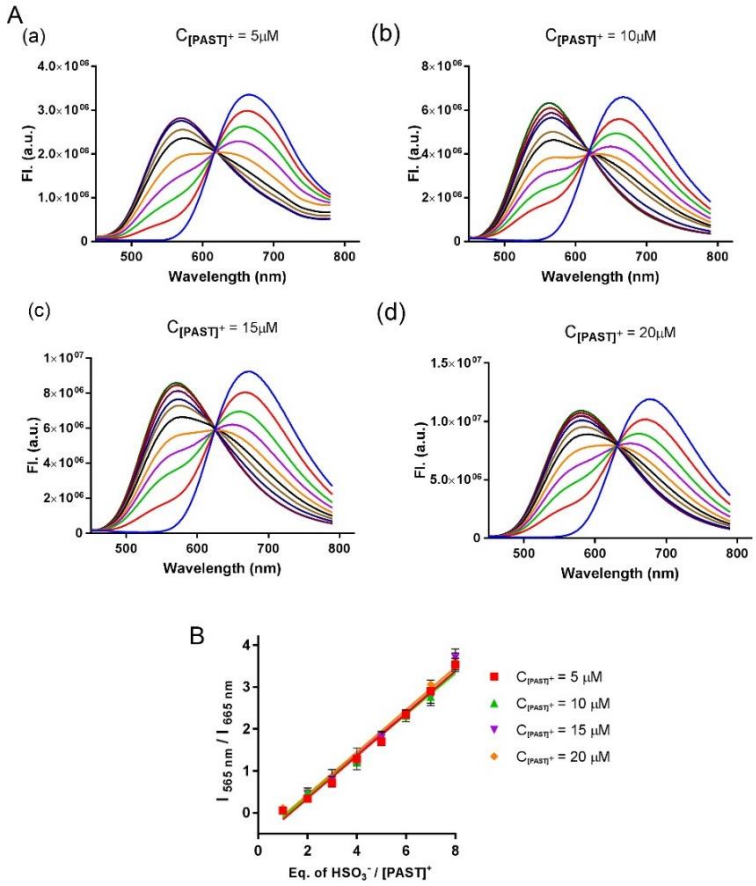

Fig. S19 A: Emission spectra of **[PAST]**$^+$ ((a): 5.0 μM; (b): 10 μM, this data comes from Fig. 1E in the manuscript.; (c): 15 μM; (d): 20 μM) upon HSO_3^- titration in DNA enrichment buffer solution, respectively, (the HSO_3^- concentration for (a): 0 - 50μM, for (b): 0 - 100μM, for (c): 0 - 150μM, for (d): 0 - 200μM). B: Linear relationship between the the changes of $I_{565\ nm}/I_{665\ nm}$ emission ratio (λ_{ex} = 405 nm) and equivalents of HSO_3^- /**[PAST]**$^+$, the data were collected from Fig. S19: A.

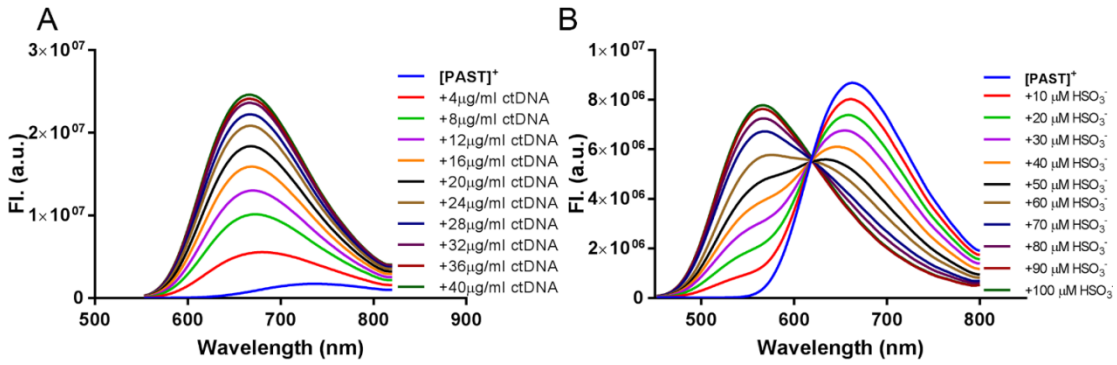

Fig. S20 (A) Fluorescence spectra of **[PAST]**$^+$ (10 μM, λ_{ex} = 515 nm) in PBS solution with increasing concentrations of ctDNA (up to 40 μg/mL); (B) Fluorescence response of **[PAST]**$^+$ (10 μM, λ_{ex}=405 nm) toward different concentrations of $NaHSO_3$ (0 - 100 μM) in PBS with 40 μg/mL of ctDNA.

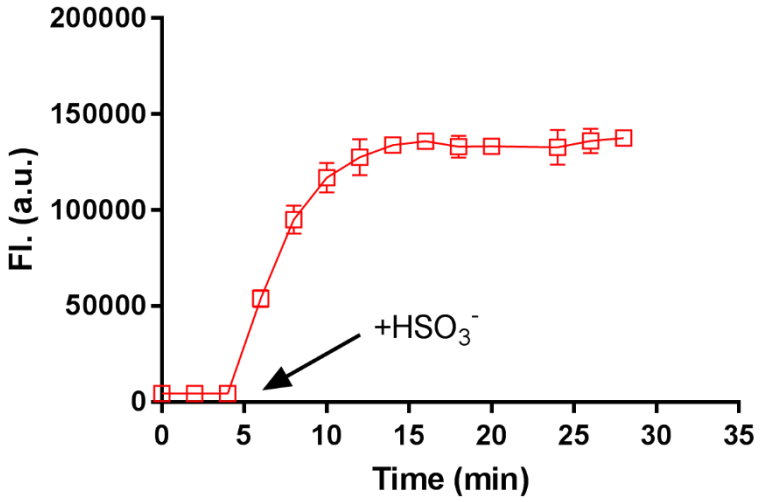

Fig. S21 Time course of the fluorescence response of **[PAST]**$^{+}$ (10 μM) upon addition of 100 μM of $NaHSO_3$ in DNA enrichment buffer solution (PBS with 40 μg/mL of ctDNA). $\lambda_{ex}/\lambda_{em}$= 405 nm/565 nm.

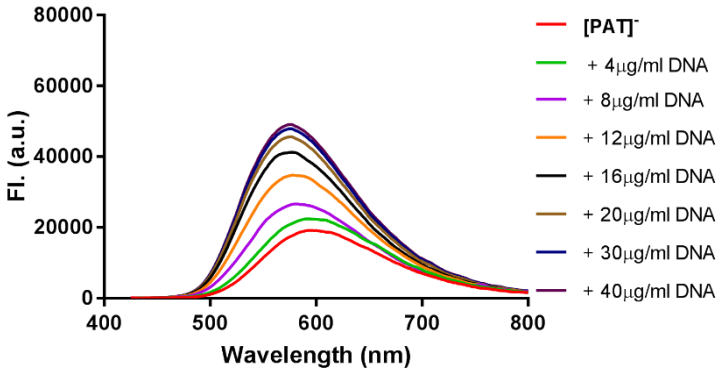

Fig. S22 Fluorescence spectra of **[PAT]**$^{-}$ (10 μM) in PBS with increasing concentrations of ctDNA (up to 40 μg/mL), λ_{ex} = 405 nm.

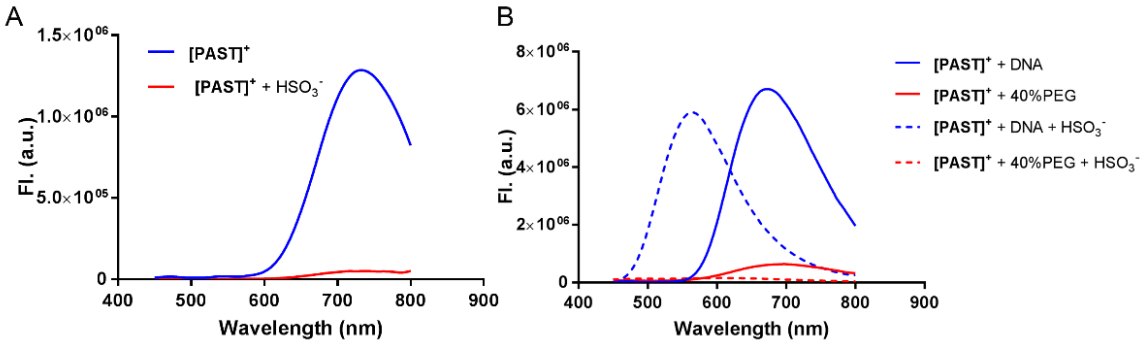

Fig. S23 (A). Fluorescence response of **[PAST]**$^{+}$ (10 μM) to $NaHSO_3$ (10 μM) in PBS; (B) Emission spectra of **[PAST]**$^{+}$ (10 μM) before (solid line) and after (dotted line) addition of 100 μM of $NaHSO_3$ in PBS solution containing 40% PEG (red line) or 40 μg/mL ctDNA (blue line), respectively, λ_{ex} = 405 nm.

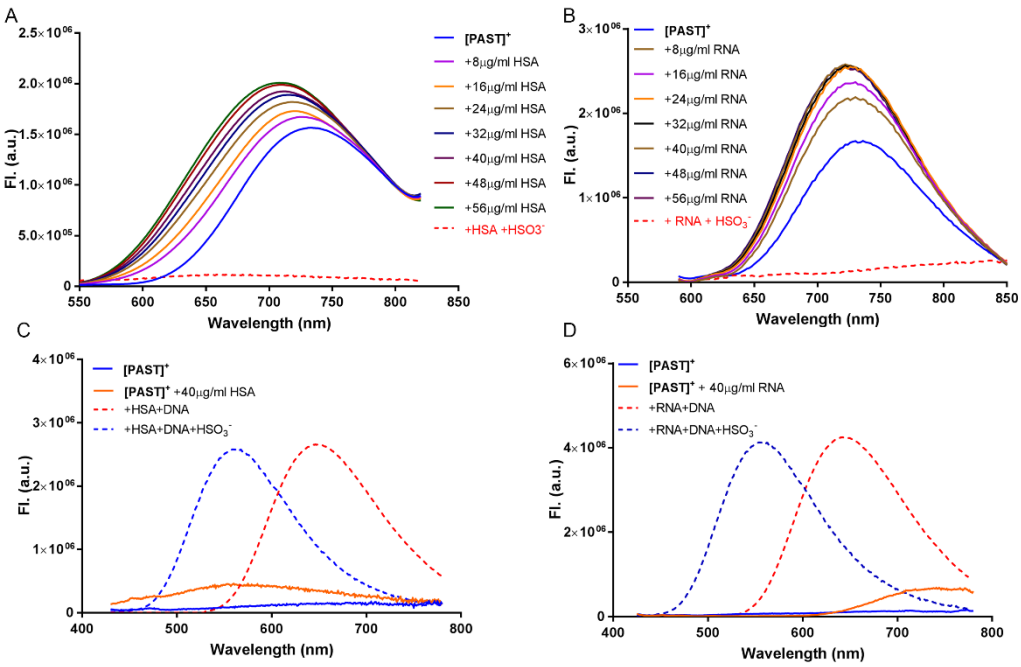

Fig. S24 (A-B) Fluorescence spectra of **[PAST]**$^{+}$ (10 μM, λ_{ex} = 515 nm) in PBS solution with increasing concentrations of HSA and RNA (up to 56 μg/mL), respectively. At the end of HSA/RNA titration (56 μg/mL), 100 μM of $NaHSO_3$ was added, inducing significantly decrease of the fluorescence, as indicated by the dotted red line; (C-D) Fluorescence response of **[PAST]**$^{+}$ (10 μM, λ_{ex} = 405 nm) toward 100 μM of $NaHSO_3$ of $NaHSO_3$ (0-100 μM) in PBS with 40 μg/mL of HSA/RNA compared with that in PBS with 40 μg/mL of ctDNA.

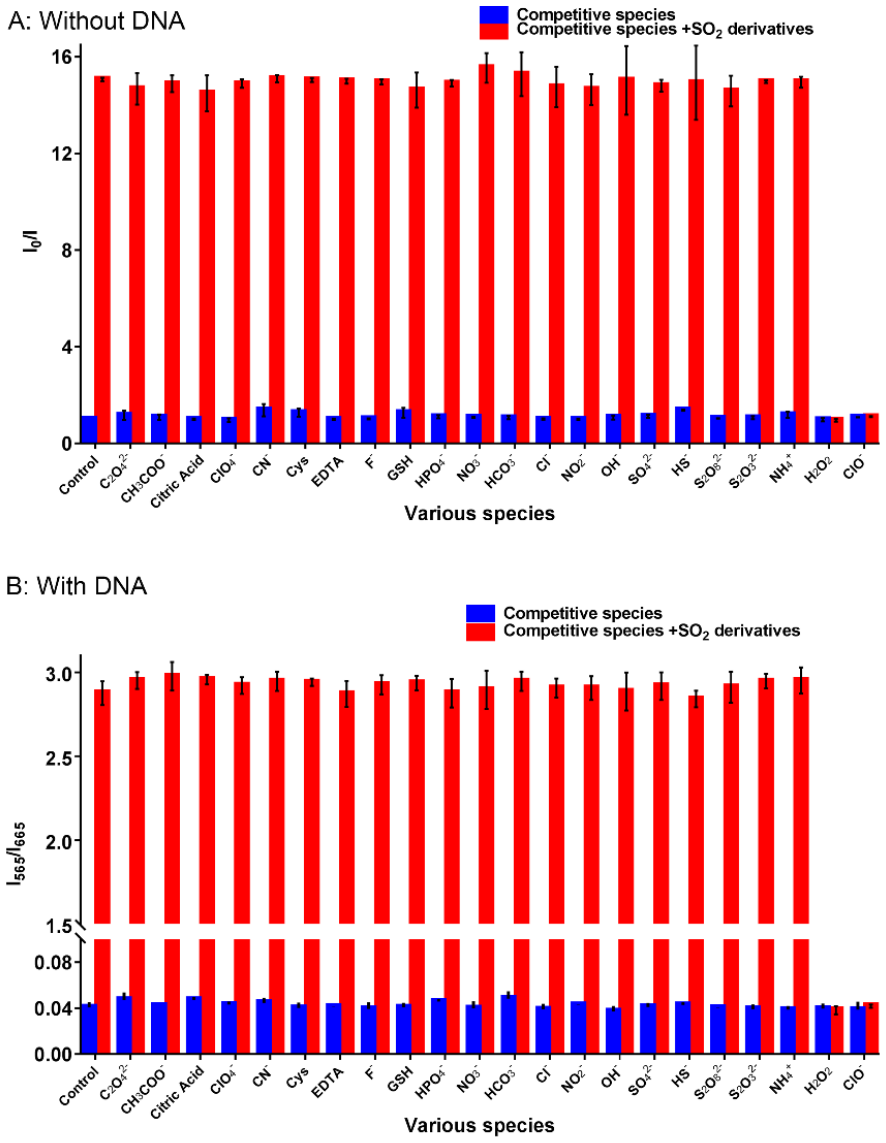

Fig. S25 Fluorescence response of **[PAST]**$^{+}$ (10 μM) to SO_2 derivatives in the presence of various relevant analytes (2.0 mM) in PBS (λ_{ex} / λ_{em} = 515 nm/735 nm) (A) and DNA enrichment buffer solution (λ_{ex} /λ_{em} = 405 nm/665 nm) (B), respectively. The fluorescence response of **[PAST]**$^{+}$ toward SO_2 derivatives was not observed in the presence of a large amount of H_2O_2 and ClO^-, which was reliable because these two species could react with HSO_3^- /SO_3^{2-}).

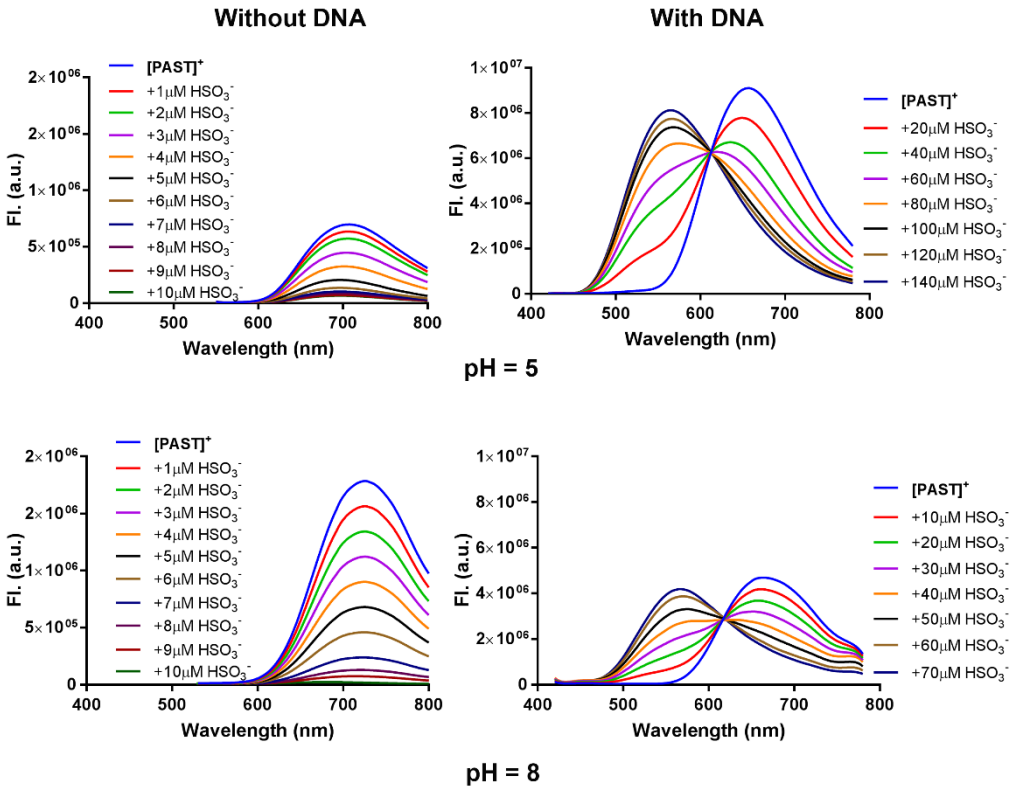

Fig. S26 Fluorescence response of **[PAST]**$^{+}$ (10 μM) to SO_2 derivatives in PBS with or without 40 μg/mL ctDNA (λ_{ex} = 405 nm) at pH=5 and pH=8.

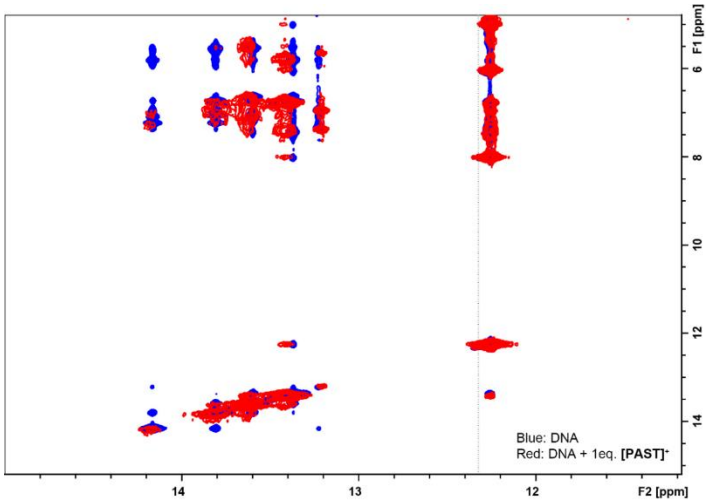

Fig. S27 The superposition of the 2D H-H NOESY spectra of dsDNA in PBS with or without **[PAST]**$^{+}$, pH =7.4, at 5 °C.

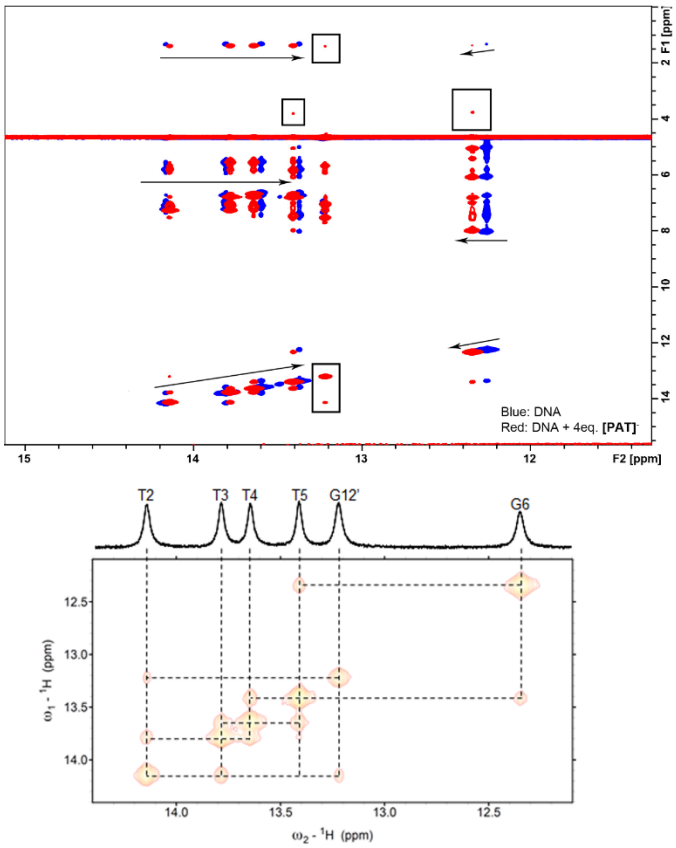

Fig. S28 The superposition of the 2D H-H NOESY spectra of dsDNA with or without **[PAT]**$^{-}$, pH =7.4, at 5 °C.

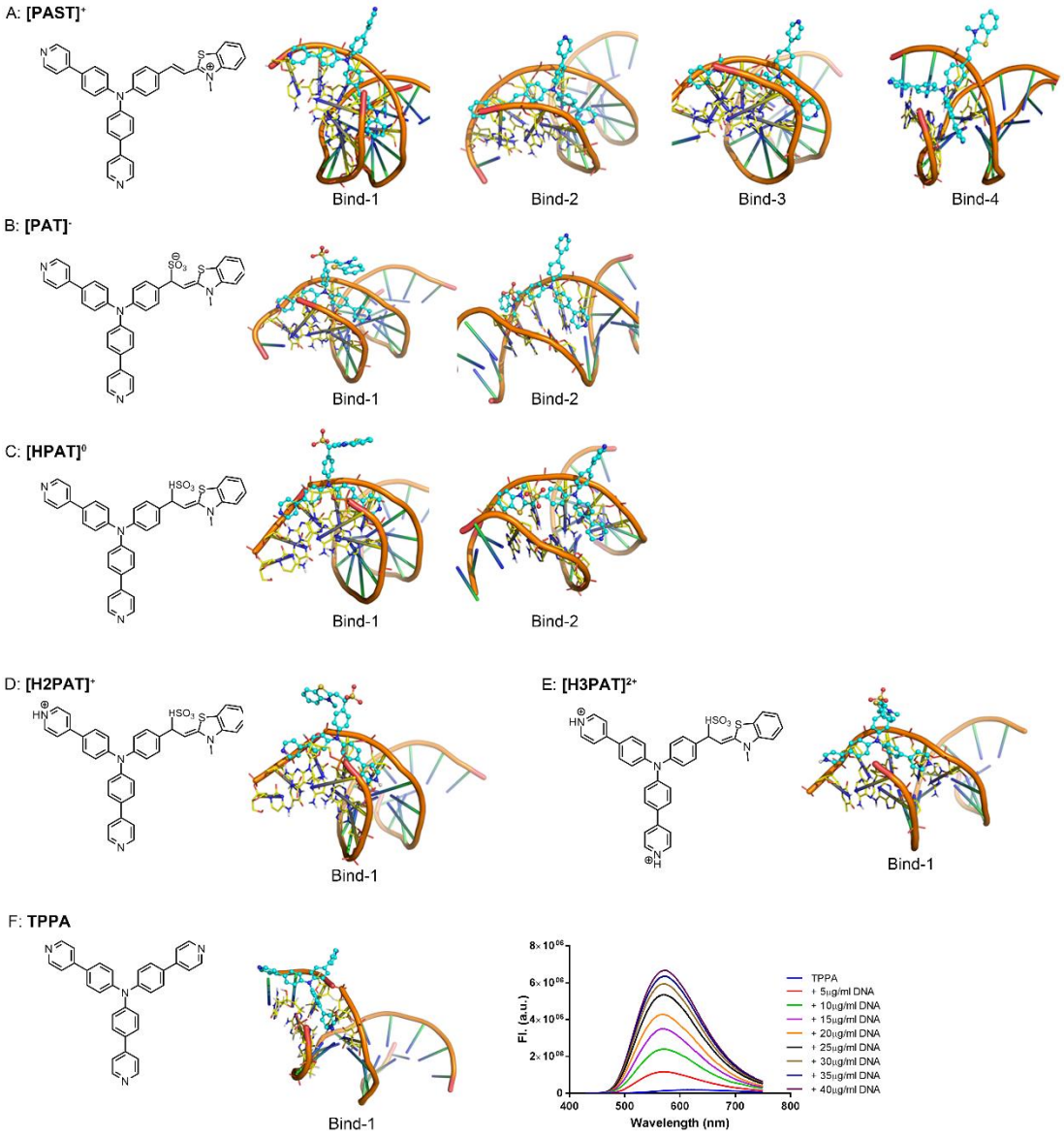

G:

Compounds	Bind-1 *(kcal/mol)*	Bind-2 *(kcal/mol)*	Bind-3 *(kcal/mol)*	Bind-4 *(kcal/mol)*
[PAST]$^{+}$	-36.7	-32.3	-34.0	-17.3
[PAT]$^{-}$	-11.1	-2.9	-0.8 (dissociated)	0.6 (dissociated)
[HPAT]^{0}	-11.8	-0.9 (dissociated)		
[H2PAT]$^{+}$	-20.4			
[H3PAT]$^{2+}$	-21.5			
TPPA	-16.7			

Fig. S29 The highest scored models of (A) **[PAST]$^{+}$**, (B) **[PAT]$^{-}$**, (C) neutral **[HPAT]^{0}**, (D) positively charged **[H_2PAT]$^{+}$**, (E) **[H_3PAT]$^{2+}$**, and control compound **TPPA** possessing symmetric structure respectively, docking to the same narrow groove of a 12-mer duplex DNA fragment. The nucleotides T_2, T_3, T_4, T_5, A_{21}, A_{22} and A_{23} were colored in

blue/yellow and highlighted in stick model. The fluorescence spectra of TPPA in PBS with increasing concentrations of ctDNA is also shown in (F). (G) The binding energies of different DNA binding modes of these compounds.

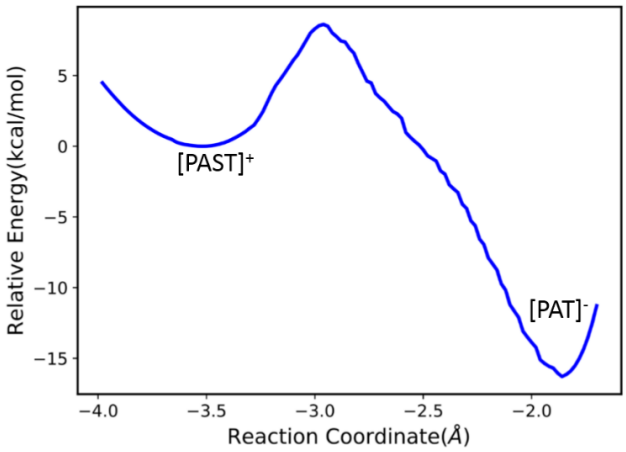

Fig. S30 The potential energy surface of the sulfite ion addition reaction.

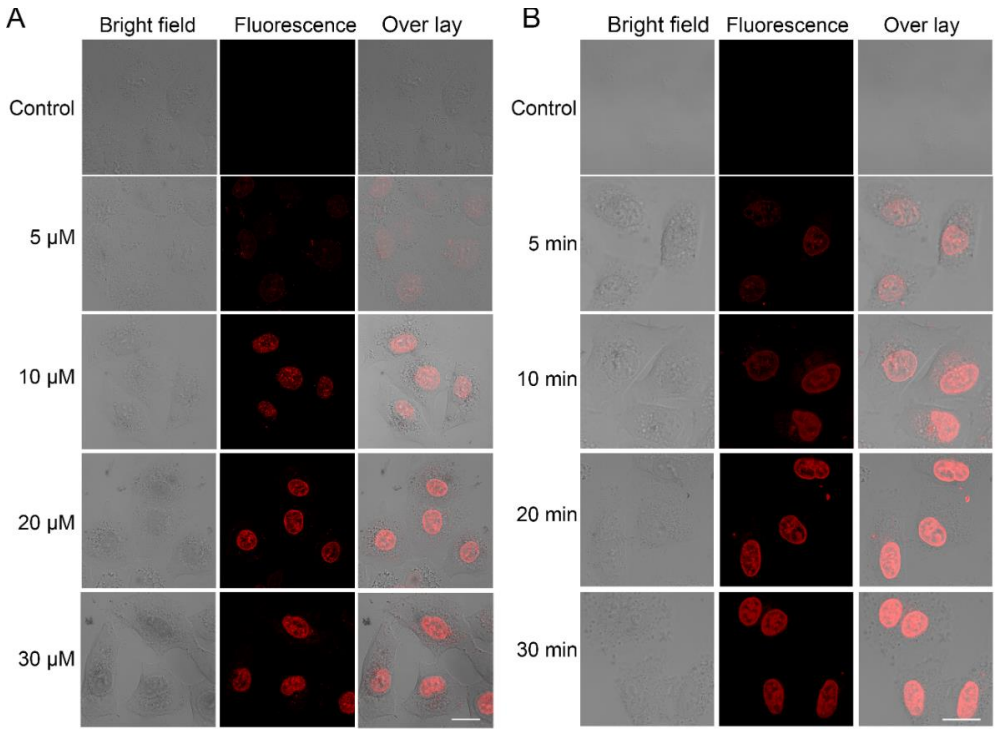

Fig. S31 Confocal fluorescence images of A549 cells. (A) A549 cells were incubated with different concentrations of **[PAST]**$^{+}$ (5 μM,10 μM, 20 μM and 30 μM) for 30 min; (B) Cells were incubated with 20 μM of **[PAST]**$^{+}$ and measured every 5/10 mins. The **[PAST]**$^{+}$ was excited at 543 nm. The emission was collected at 665 ± 20 nm. Scale bar: 20 μm.

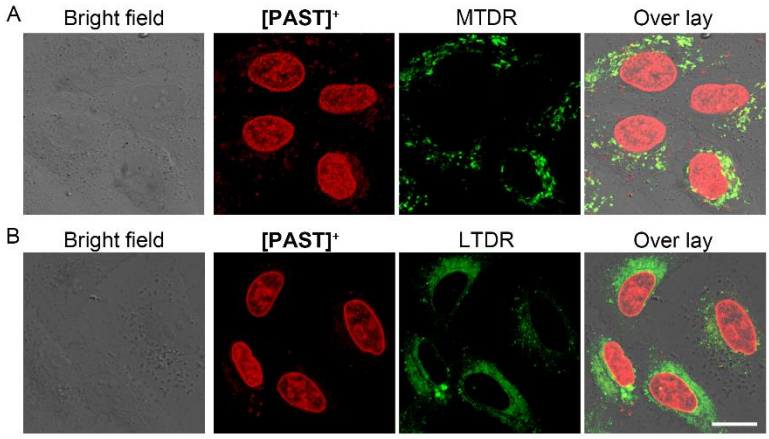

Fig. S32 Confocal fluorescence images of A549 cells co-labeled with **[PAST]**$^{+}$ (20 μM, 20min) and MTDR (MitoTracker Deep Red) (100 nM, 30min) (A); LTDR (LysoTracker Deep Red) (100 nM, 30min) (B).

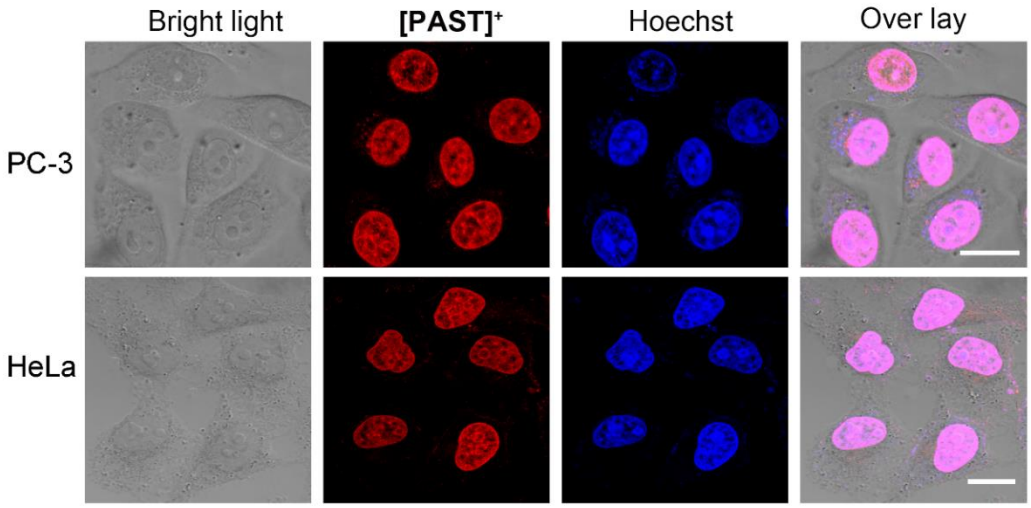

Fig. S33 Confocal fluorescence images of PC-3 and Hela cells co-labeled with **[PAST]**$^{+}$ (20 μM, 20min) and Hoechst (Hoechst 33342) (150 nM, 30min).

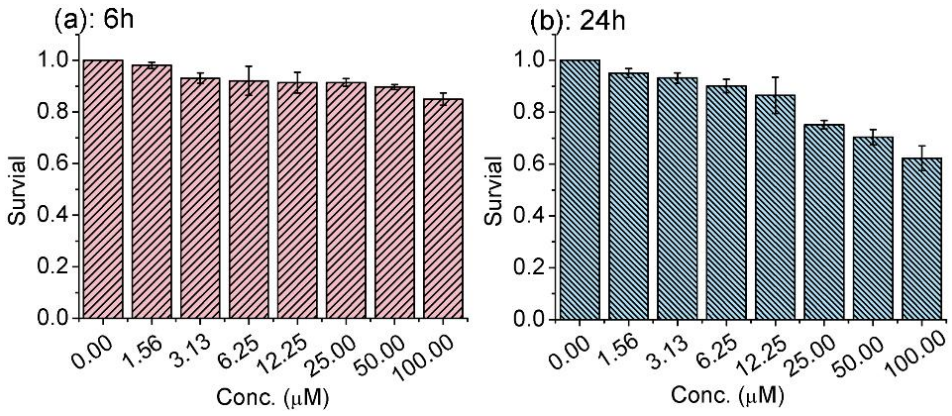

Fig. S34 Viability of A549 cells treated with different concentrations of **[PAST]**$^{+}$ for 6h and 24h.

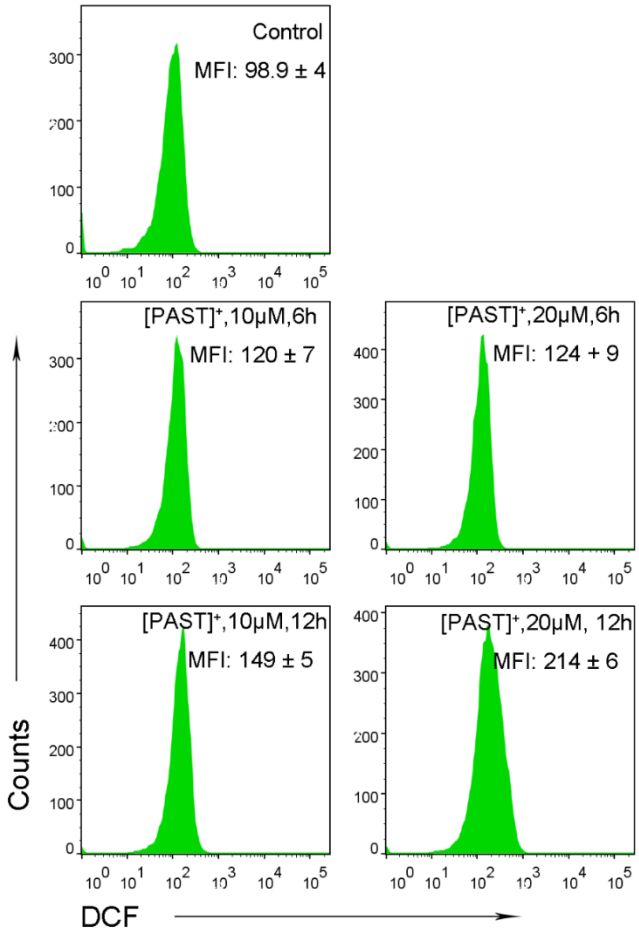

Fig. S35 Analysis of ROS levels by flow cytometry after A549 cells were treated with vehicle or **[PAST]**$^{+}$ at the indicated concentrations for 6/12h and stained with DCFH-DA.

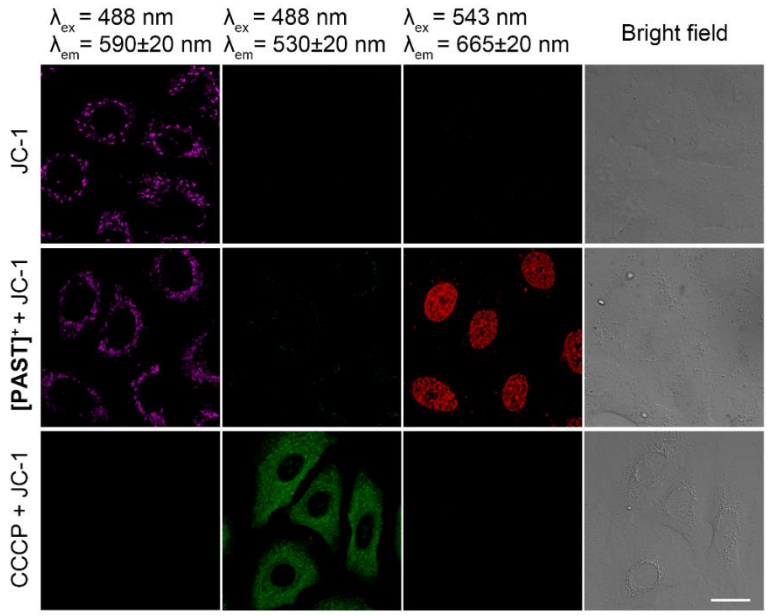

Fig. S36 Effects of **[PAST]**$^{+}$ on MMP analyzed by JC-1 staining and confocal fluorescence images. A549 cells were treated with vehicle or **[PAST]**$^{+}$ (20 μM) at the indicated concentrations for 6 h. A commercial drug can induce mitochondrial apoptosis CCCP as positive control.

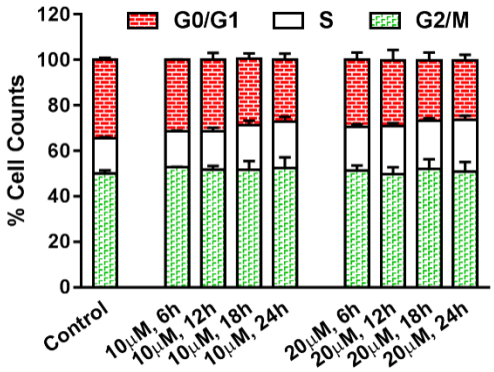

Fig. S37 Concentration-dependent and time-dependent effects of **[PAST]**$^{+}$ on cell cycle distribution of A549 cells after treatment for different times. Cells were analyzed for DNA content by flow cytometry after PI staining.

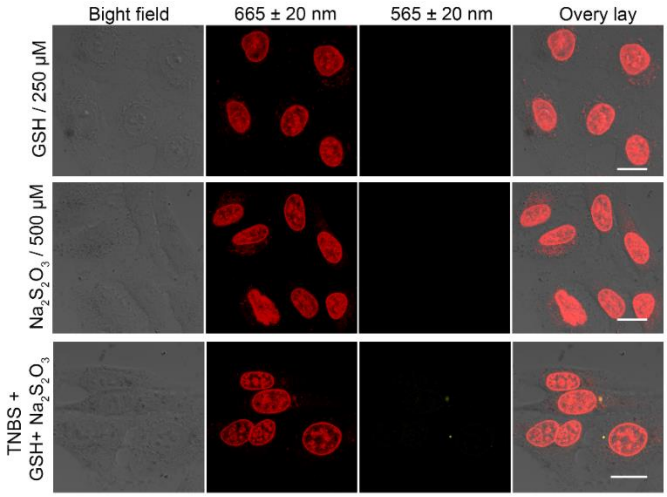

Fig.S38 Ratiometric fluorescence imaging of endogenous SO_2 derivatives in the nucleus of living cells. A549 cells were incubated with **[PAST]**$^+$(10 μM) for 20 min and then treated with GSH (250 μM, 30min, upper panel)or thiosulphate (500 μM, 30 min, middle panel), respectively; A549 cell in lower panel were pre-treated with TNBS (a thiosulphate sulphurtransferase inhibitor, 1 mM, 2 h) before thiosulphate/GSH (500 μM /250 μM, 30 min) simulation. Scale bar: 20 μm.

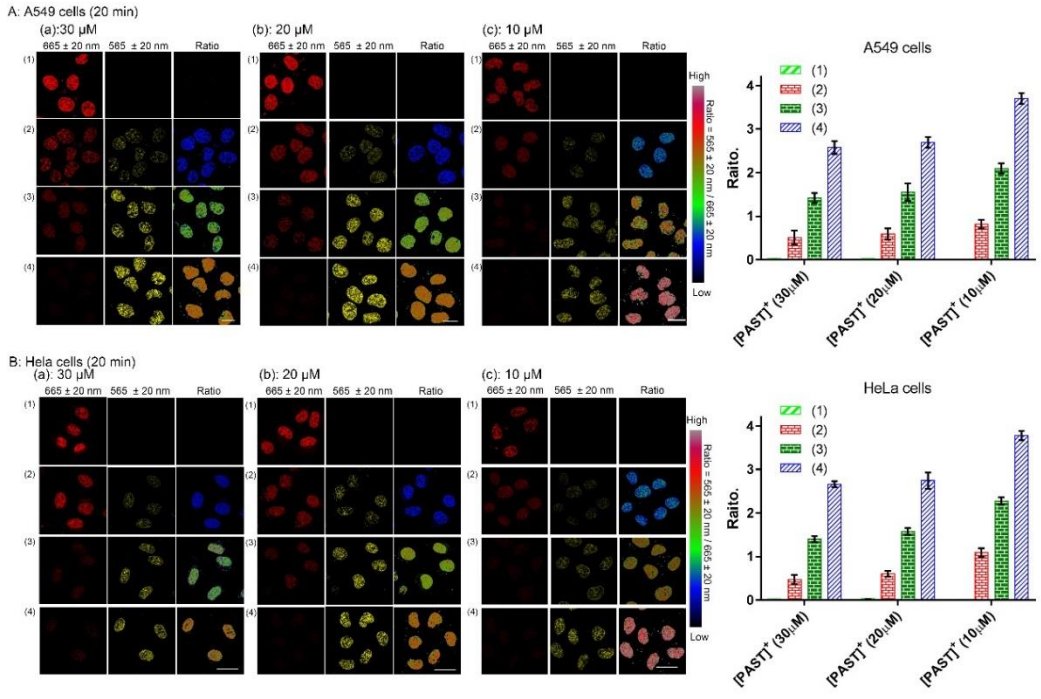

Fig. S39 Ratiometric fluorescence imaging of the variations of endogenous SO_2 derivatives in the nucleus of A549 cells (A) and HeLa cells (B). Cells were incubated with **[PAST]**$^+$ (30 μM) (a), (20 μM) (b) and (10 μM) (c) for 20 min and then treated with

thiosulphate / GSH at (1) 0 μM / 0 μM (control), (2) 120 μM / 60 μM, (3) 240 μM /120 μM, and (4) 300 μM /150 μM for another 30 min to stimulate endogenous SO_2 derivatives; Scale bar: 20 μm. (The data of Fig. S39 A(b) comes from Fig. 3 in the manuscript.) The ratio of fluorescence photons number collected from the red and yellow channel, each data was calculated from 3-5 fields of view and each experimental condition was performed in triplicate.

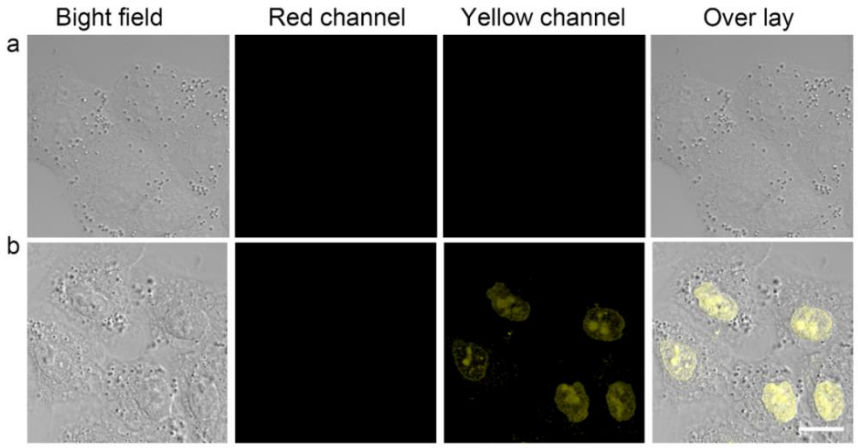

Fig. S40 (A) Confocal images of living cells incubated with **[PAT]**$^-$ (20 μM, 20 min); (B) Living cells were incubated with **[PAT]**$^-$ (20 μM, 20 min) followed with PBS washing, culture medium refreshing, and cell permeation. Scale bar: 20 μm.

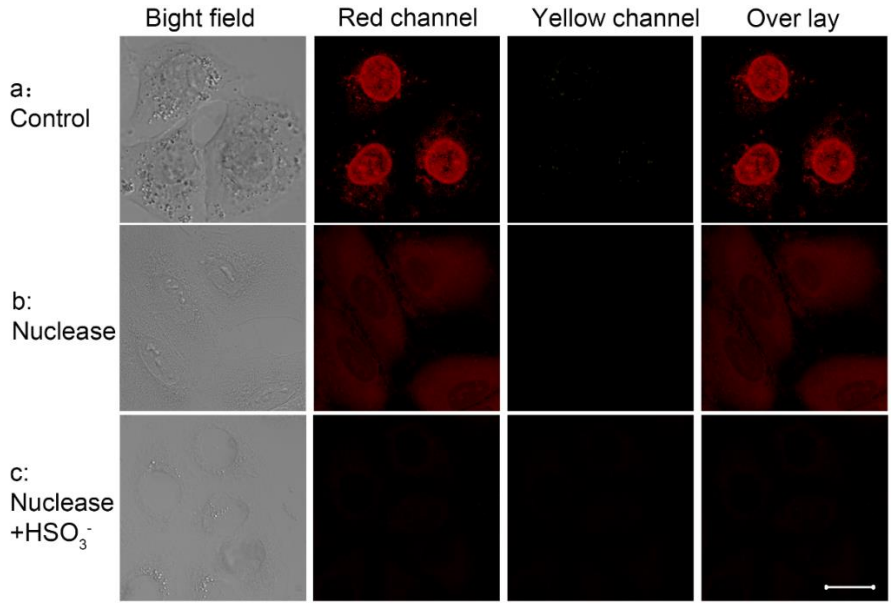

Fig. S41 Nuclease digest experiments of **[PAST]**$^+$ (20 μM) in A549 cells (shown as comparison experiments). Scale bar: 20 μm.

Table S1. Crystallographic data of **[PAST]$^+$**

Compound	**[PAST]$^+$**
CCDC NO.	1893794
formula	$C_{39}H_{31}Cl_2IN_4S$
molecular weight	785.56
description	block, metallic reddish red
temperature (K)	150
crystal size (mm)	0.10 × 0.10 × 0.10
λ (Å)	1.54178
crystal system	triclinic
space group	P -1
a (Å)	9.9365(3)
b (Å)	10.4295(3)
c (Å)	18.8256(5)
α (o)	94.895(2)
β (o)	96.163(2)
γ (o)	115.854(3)
volume, Å	1726.38(9)
Z	2
absorption coefficient (mm^{-1})	9.542
F(000)	792.0
θ range (deg)	7.3 - 123.3
reflections collected/unique	5697
final R indices[$I > 2\sigma(I)$][a]	R_1 = 0.0583, wR_2 = 0.1816
R indices (all data)	R_1 = 0.0628, wR_2 = 0.1853
GOF[b]	1.194

Table S2 Selected bond Lengths for **[PAST]**$^{+}$.

	Bond Length (Å)		**Bond Length (Å)**
S1-C3	1.713(8)	N3-C20	1.339(13)
S1-C38	1.745(8)	N2-C10	1.343(15)
N4-C31	1.351(10)	N2-C9	1.335(15)
N4-C33	1.411(10)	C25-C26	1.407(10)
N4-C32	1.423(10)	C30-C31	1.428(10)
N1-C1	1.429(10)	C30-C29	1.360(11)
N1-C23	1.409(10)	C26-C27	1.396(11)
N1-C12	1.410(9)	C26-C29	1.437(10)
N3-C21	1.325(12)		

Table 3 Selected bond angles (deg) for **[PAST]**$^{+}$

	Angle/˚		**Angle/˚**
C31-S1-C38	91.3(4)	C6-C1-N1	120.1(7)
C31-N4-C33	113.1(6)	N4-C31-S1	112.9(5)
C31-N4-C32	125.0(6)	N4-C31-C30	124.7(7)
C33-N4-C32	121.7(6)	C30-C31-S1	122.5(6)
C23-N1-C1	119.7(6)	C30-C29-C26	129.3(7)
C23-N1-C12	123.0(6)	N3-C20-C19	123.7(8)
C12-N1-C1	116.5(6)	C40-C33-N4	112.3(7)
C21-N3-C20	115.8(7)	C34-C33-N4	127.0(8)
C9-N2-C10	115.7(9)	N1-C23-C28	119.2(7)
N3-C21-C22	125.3(8)	C24-C23-N1	122.5(7)
C29-C30-C31	119.6(7)	C37-C40-S1	127.7(8)
C2-C1-N1	120.7(7)	N2-C10-C11	123.6(10)
C33-C40-S1	110.4(6)	N2-C9-C8	125.1(10)
C17-C12-N1	121.8(7)	C13-C12-N1	119.5(7)

Table S4. Photophysical data of **[PAST]**$^{+}$ and **[PAT]**$^{-}$(10 μM) at room temperature.

Compounds	Solvent	λ_{abs} (nm)	ε_{max} (10^4 cm^{-1} mol^{-1} L)	λ_{em} (nm)	Φ_{PL}[a] (%)	τ[b] (ns)
[PAST]$^+$	PBS	515/345	2.869	735	0.896	1.01
	CH_3OH	514/351	4.201	732	0.419	0.434
	CH_2Cl_2	551/348	5.327	736	0.941	0.419
[PAT]$^-$	PBS	351	2.109	575	0.067	1.73
	CH_3OH	366	3.438	476	0.017	1.07
	CH_2Cl_2	348	3.861	534	0.028	1.45
DNA-**[PAST]$^+$**	PBS	509/371	2.956	665	10.536	1.59
DNA-**[PAT]$^-$**	PBS	432	2.602	565	7.523	1.81

a: Quantum yields of luminescence at room temperature were calculated according to literature procedures[12]. Solutions of rhodamine 6G and coumarin 307 were used as the standard.

b: Decay curves of compounds were recorded by an Edinburgh FLS 920 Spectrometer. The lifetimes were measured at the emission maxima.

Reference:

[1]. Gaur, P.*, et al.* Selenium Incorporated Cationic Organochalcogen: Live Cell Compatible and Highly Photostable Molecular Stain for Imaging and Localization of Intracellular DNA. *ACS Appl. Mater. Inter.* 8, 10690-10699 (2016).

[2]. Lefebvre, J.-F., Sun, X.-Z., Calladine, J.A., George, M.W. & Gibson, E.A. Promoting charge-separation in p-type dye-sensitized solar cells using bodipy. *Chem. Commun. (Camb)* 50, 5258-5260 (2014).

[3]. Wu, J.W.*, et al.* Dipyridylphenylamine-based chemodosimeter for sulfite with optimizing ratiometric signals via synchronous fluorescence spectroscopy. *Dyes Pigments* 136, 175-181 (2017).

[4]. Jorgensen, W.L., Chandrasekhar, J., Madura, J.D., Impey, R.W. & Klein, M.L. Comparison of simple potential functions for simulating liquid water. *J. Chem. Phys.* 79, 926-935 (1983).

[5]. Frisch*, et al.* Gaussian Inc. Gaussian 09, Revision A.1. *Wallingford CT* (2009).

[6]. Christopher I. Bayly, P.C., Wendy D, Cornell, Peter A. Kollman. A well-behaved electrostatic potential based method using charge restraints for deriving atomic charges: the RESP model. *J. Phys. Chem.* 97, 10269-10280 (1993).

[7]. Gotz, A.W*., et al.* Routine Microsecond Molecular Dynamics Simulations with AMBER on GPUs. 1. Generalized Born. *J. Chem. Theory Comput.* 8, 1542-1555 (2012).

[8]. Ryckaert, J.-P., Ciccotti, G. & Berendsen, H.J.C. Numerical integration of the cartesian equations of motion of a system with constraints: molecular dynamics of n-alkanes. *Journal of Computational Physics* 23, 327-341 (1977).

[9]. Friesner, R.A*., et al.* Extra precision glide: docking and scoring incorporating a model of hydrophobic nclosure for protein-ligand complexes. *J. Med. Chem.* 49, 6177-6196 (2006).

[10]. Zhou, R.H., Harder, E., Xu, H.F. & Berne, B.J. Efficient multiple time step method for use with Ewald and particle mesh Ewald for large biomolecular systems. *J. Chem. Phys.* 115, 2348-2358 (2001).

[11]. Kolanowski, J. C, Shen, New, E. J. Fluorescent probes for the analysis of labile metals in brain cells, *Metals in the Brain: Measurement and Imaging, Neuromethods*, 124, (2017).

[12]: Crosby G A, Demas J N. Measurement of photoluminescence quantum yields. Review. J. Phys. Chem. 75: 991-1024, (1971).